Investigation on Optical and Biological Properties of 2-(4-Dimethylaminophenyl)benzothiazole Based Cycloplatinated Complexes

Rebeca Lara,[a] Gonzalo Millán,[a] M. Teresa Moreno,[a] Elena Lalinde,*[a] Elvira Alfaro-Arnedo,[b] Icíar P. López,[b] Ignacio M. Larráyoz,*[c] and José G. Pichel*[b, d]

Abstract: The optical and biological properties of 2-(4-dimethylaminophenyl)benzothiazole cycloplatinated complexes featuring bioactive ligands ([{Pt(Me_2N-pbt)(C_6F_5)}L] [L = Me_2N-pbtH **1**, *p*-dpbH (4-(diphenylphosphino)benzoic acid) **2**, *o*-dpbH (2-(diphenylphosphino)benzoic acid) **3**), [Pt(Me_2N-pbt)(*o*-dpb)] **4**, [{Pt(Me_2N-pbt)(C_6F_5)}$_2$(μ-PR_nP)] [PR_4P = O-($CH_2CH_2OC(O)C_6H_4PPh_2$)$_2$ **5**, $PR_{12}P$ = O{(CH_2CH_2O)$_3$C(O)$C_6H_4PPh_2$}$_2$ **6**] are presented. Complexes **1**–**6** display ^{1}ILCT and metal-perturbed ^{3}ILCT dual emissions. The ratio between both bands is excitation dependent, accomplishing warm-white emissions for **2**, **5** and **6**. The phosphorescent emission is lost in aerated solutions owing to photoinduced electron transfer to $^3O_2$ and the formation of $^1O_2$, as confirmed in complexes **2** and **4**. They also exhibit photoinduced phosphorescence enhancement in non-degassed DMSO due to local oxidation of DMSO by sensitized $^1O_2$, which causes a local degassing. Me_2N-pbtH and the complexes specifically accumulate in the Golgi apparatus, although only **2**, **3** and **6** were active against A549 and HeLa cancer cell lines, **6** being highly selective in respect to nontumoral cells. The potential photodynamic property of these complexes was demonstrated with complex **4**.

Introduction

Since the serendipitous discovery of cisplatin antitumor activity,[1] research into the development of new platinum-based drugs focused not only on systems having similar architecture but also on different architectures and different oxidation states has been very active.[2] Furthermore, aiming to overcome the drawbacks (e.g., nephrotoxic side effects) and chemoresistance of the clinically established platinum antitumor agents (cisplatin, carboplatin and oxalaplatin),[3] research has been also shifting to multimetallic systems,[4] to other metal ions[5] and to the incorporation of different organic molecules into metal complexes to form drugs with dual activity.[2d,h,6] Several reviews cover different aspects of these complexes, including strategies based on biologically targeting groups,[2d,h,6] photoactivated complexes[7] or recent progress in the application of tumor targeting groups,[2d,6b] nanostructures for selective release mechanisms[2f,8] or simultaneously acting as co-delivery and agent for imaging.[9]

The mechanism of action of many cisplatin-like anticancer drugs mainly relies on nuclear crosslink DNA,[2b,c] although other complexes are known to stablish noncovalent interactions such as electrostatic, groove binding or π-stacking, ultimately leading to apoptosis in fast-dividing cells.[2c,10] Interactions of Pt complexes with cytoplasmic nucleophiles, including mRNA,[2g,11] as well as, multiple mitochondrial and extra mitochondrial proteins,[4a,6d,12] which induce oxidative and reticular stress damage responses, have also been reported. Specifically, enzyme inhibition was a recently disclosed significant and alternative mechanism for Pt-based anticancer therapeutics.[6c,13]

Concerning new metal-based antineoplastic agents development, improving its biological properties in terms of cellular selectivity and therapeutic efficiency reducing side effects is doubtlessly a crucial factor. In this context, the rational design of luminescent complexes able of accumulating or interact with different cellular organelles acting as molecular probes for cellular imaging or as new trackable anticancer drugs has become one of the prime research interest for the last decade.[9b–e,14] Among the various luminescent transition metals,

[a] Dr. R. Lara, G. Millán, Prof. Dr. M. T. Moreno, Prof. Dr. E. Lalinde
Departamento de Química-Centro de Síntesis Química de La Rioja, (CISQ)
Universidad de La Rioja
26006 Logroño (Spain)
E-mail: elena.lalinde@unirioja.es

[b] E. Alfaro-Arnedo, Dr. I. P. López, Dr. J. G. Pichel
Lung Cancer and Respiratory Diseases Unit (CIBIR)
Fundación Rioja Salud
26006 Logroño (Spain)
E-mail: jgpichel@riojasalud.es

[c] Dr. I. M. Larráyoz
Biomarkers and Molecular Signaling Unit (CIBIR)
Fundación Rioja Salud
26006 Logroño (Spain)
E-mail: ilarrayoz@riojasalud.es

[d] Dr. J. G. Pichel
Biomedical Research Networking Center in Respiratory Diseases (CIBERES)
ISCIII
Av. Monforte de Lemos, 3-5. Pab. 11. 28029 Madrid (Spain)

Supporting information for this article is available on the WWW under https://doi.org/10.1002/chem.202102737

square planar cycloplatinated complexes represent a particularly interesting group because of their efficient phosphorescence with tunable emission color, and long-lived emissive excited states.[7a,9a,15] In addition, their strong propensity to form noncovalent π–π and Pt–Pt interactions endows supramolecular nanostructures,[16] which usually exhibit enhanced red-shifted emissions, with interesting applications in different fields, including biological organelle monitoring.[9a,15]

Despite the extraordinary growth of phosphorescent cycloplatinated complexes studies,[17] reporting on their potential biomedical applications are still rather limited.[18] In this regard, the presence of strong σ (M–C) bonds associated to a more or less π-extended cyclometalated framework enhances the complex stability and their planarity promotes typical intercalation processes with DNA[10a–d] or with telomeric G-quadruplex,[14a,18d,19] which can be tracked with fluorescence or confocal microscopy. The auxiliary ligands could be selected to induce simultaneously covalent binding, which can be favored by the strong *trans*-effect of the metalated C atom. For instance, Tunik, Chou and co-workers have recently reported the selective coordination of a cycloplatinated fragment to the histidine residue of ubiquitin to form {[Pt(ppy)(PPh_3)]/ubiquitin} conjugates, with concomitant switch-on of strong emission upon interaction of the Pt fragment with the imidazole function.[20]

Designing transition metal complexes with selective and specificity toward a particular organelle, which is a crucial factor in the development of next generation metal-based drugs, is also a challenging task. Indeed, targeting a different organelle instead of the nucleus is an alternative approach to improve the efficacy of a drug, thus overcoming typical resistance caused by nucleotide excision repair mechanism.[2d,5a,6a,21] In this context, the structural framework of cycloplatinated complexes could also be tailored through substituent modification to satisfy the requirements of an organelle-targeting drug. Finally, it is worth mentioning that in case of lack of activity in the dark these phosphorescent complexes, exhibiting suitable charge transfer ^{3}ILCT, ^{3}MLCT or ^{3}LLCT excited states, can also be exploited as photosensitizers to induce reactive oxygen species.[22]

Benzothiazole is a central structure of diverse natural compounds and of many other small organic molecules with a wide range of applicability in medicinal chemistry. In particular, 2-arylbenzothiazoles have demonstrated potent antitumor activity[23] and efforts have been directed toward their use as amyloid-binding biomarkers.[24] In particular, 2-(4-dimethylaminophenyl)benzothiazole (Me_2N-pbtH), a simple molecule with donor-acceptor properties, has been extensively studied due to its facile preparation and interesting photophysical properties.[25] However, although some Ir^{III} complexes based on Me_2N-pbt have been reported and applied as yellow phosphorescent materials,[26] as far as we know, reports related to biological activity of cyclometalated complexes based on this ligand are extremely limited.[27]

In this topic, our group following our interest in platinum complexes featuring chromophoric benzothiazole units,[28] recently reported on the synthesis and intriguing photophysical properties of several [Pt(Me_2N-pbt)ClL] [L = DMSO; 1,3,5-triaza-7-phosphaadamantane (PTA); 3,3,3''-trisulfonate sodium salt (TPPTS)] related with reversible and irreversible protonation processes.[27] Bioactivity studies revealed perinuclear staining and moderate cytotoxic activity for the DMSO and PTA complexes towards the human tumor cell lines A549 and HeLa, which was suggested to be governed by inhibition of tubulin polymerization. Similar perinuclear localization with improved bioactivity was observed in pentafluorophenyl-cycloplatinated complexes [Pt(C^N)(C_6F_5)L] (C^N = ppy, dfppy) incorporating DMSO and the biocompatible phosphine 4-(diphenylphosphino)benzoic acid ($PPh_2C_6H_4COOH$, dpbH) as auxiliary ligands, whereas the lack of activity of the complexes featuring the peptide-tagged ligand $PPh_2C_6H_4CONHCH_2COOMe$ (dpbGlyOMe) was attributed to their low solubility in the biological medium.[29] Immunostaining studies with complex [Pt(dfppy)(C_6F_5)(dpbH)] on A549 and HeLa revealed that effectively have antitubulin activity more efficient in the A549 cell line.

Following our project in this topic, we decided to further investigate the optical and biological properties of new cyclometalated Pt complexes featuring the Me_2N-pbt scaffold and incorporating non-leaving carboxy-substituted phosphine ligands. Here, we disclosed that Me_2N-pbtH ligand is not intrinsically cytotoxic on human tumoral A549 cells despite its fast localization on the Golgi bodies in living cells, as revealed confocal imaging studies. Interestingly we found that their cycloplatinated complexes display also Golgi targeting selectivity. In detail, we present here the synthesis, optical properties and biological activity of new mononuclear complexes [Pt(Me_2N-pbt)(C_6F_5)L] (L = Me_2N-pbtH **1**, *p*-dpbH **2**, *o*-dpbH **3**) and [Pt(Me_2N-pbt)(*o*-dpb)] **4**. Increasing efforts have been recently devoted to improve the still limited knowledge about structure-activity correlations on homo and hetero-polynuclear complexes. Therefore, for comparative purposes, and aiming to examine the impact of the Pt units on their activity, we also present two dinuclear complexes [{Pt(Me_2N-pbt)(C_6F_5)}$_2$(μ-PR_nP)] [PR_4P = $O(CH_2CH_2OC(O)C_6H_4PPh_2)_2$ **5**; $PR_{12}P$ = $O\{(CH_2CH_2O)_3C(O)C_6H_4PPh_2\}_2$ **6**], with the Pt units connected by a diphosphine having two distinct ethylene glycol units. All complexes display intraligand fluorescence (^{1}ILCT) and metal perturbed intraligand phosphorescence (^{3}ILCT) dual emissions with a strong phosphorescence oxygen dependence. They also exhibit intriguing photoinduced phosphorescence enhancement in non-degassed DMSO, ascribed to local oxidation of DMSO to $DMSO_2$ by sensitized $^1O_2$ singlet, which remove $^3O_2$, as demonstrated in complex **2**. In contrast to the ligand Me_2N-pbtH and **1**, **4** and **5**, complexes **2**, **3** and **6** revealed cytotoxicity against A549 (lung carcinoma) and HeLa (cervix carcinoma) cancer cell lines, with higher efficiency and selective toxicity in A549 respect to nontumor 184B5 (breast epithelium) cell lines. Complex **6**, although not showing low IC_{50} values, proved to be the most selective for tumor cells. Furthermore, the potential photodynamic properties of this type of complexes was nicely demonstrated with complex **4**, which exhibited highly efficient photoinduced cytotoxicity upon a short pulse of light irradiation.

Results and Discussion

Synthesis and characterization

The synthesis of all complexes is outlined in Scheme 1 (see the Experimental Section and NMR spectra, Figures S1–S9, in the Supporting Information). Complex [Pt(Me_2N-pbt)(C_6F_5)(Me_2N-pbtH)] **1** was prepared following a previous method reported for similar pentafluorophenyl cycloplatinated complexes.[28b,30] Briefly, Me_2N-pbtH was used to prepare the precursor *cis*-[Pt(C_6F_5)$_2$(Me_2N-pbtH)$_2$], that was then refluxed in toluene for 10 h to yield **1** as a yellow solid in a very high yield.

Its spectroscopic data confirm that the isomer formed has a *cis*-C_{met},C_Rf configuration as previously found for related complexes.[28b,30] Complexes **2**, **3**, **5** and **6** were synthesized by easy displacement of Me_2N-pbtH in the cyclometalated complex **1** by the corresponding phosphines *p*-dpbH and *o*-dpbH (**2**, **3**) or diphosphines PR_4P and $PR_{12}P$ (**5**, **6**). The 4- and 2-(diphenylphosphino)benzoic acid ligands were selected because previous studies in Pt, Ru and Au complexes have demonstrated that the presence of carboxylic groups improved antitumor efficacy.[31] The synthesis of the diphosphines (PR_4P and $PR_{12}P$) have been recently reported by Dyson et al. to assess the impact of the linker length on the cytotoxicity of dinuclear Ru^{II} and Au^{I} complexes.[31]

Biological tests for water insoluble compounds often rely on the use of DMSO, therefore due to their further biological studies we examined the stability of the complexes in solution. The mononuclear complex **2** and the bimetallic **5** and **6** are stable not only in $CDCl_3$ but also in [D_6]DMSO as assessed by NMR monitoring. Not unexpectedly, for complex **1** the Me_2N-pbtH was easily substituted by DMSO leading to the solvated complex [Pt(Me_2N-pbt)(C_6F_5)DMSO], as confirmed by NMR, but the attempts to isolate this complex as a solid from the solution were unsuccessful. By contrast, in complex **3**, the presence of the COOH group in the *ortho* position causes a remarkable congestion around the Pt, which is evidenced in the static coordination of the C_6F_5 ring, exhibiting five fluorine resonances in the $^{19}F\{^1H\}$ NMR spectrum and broaden ^1H resonances due to the aromatic phenyl rings of coordinated *o*-dpbH (Figure S3b).

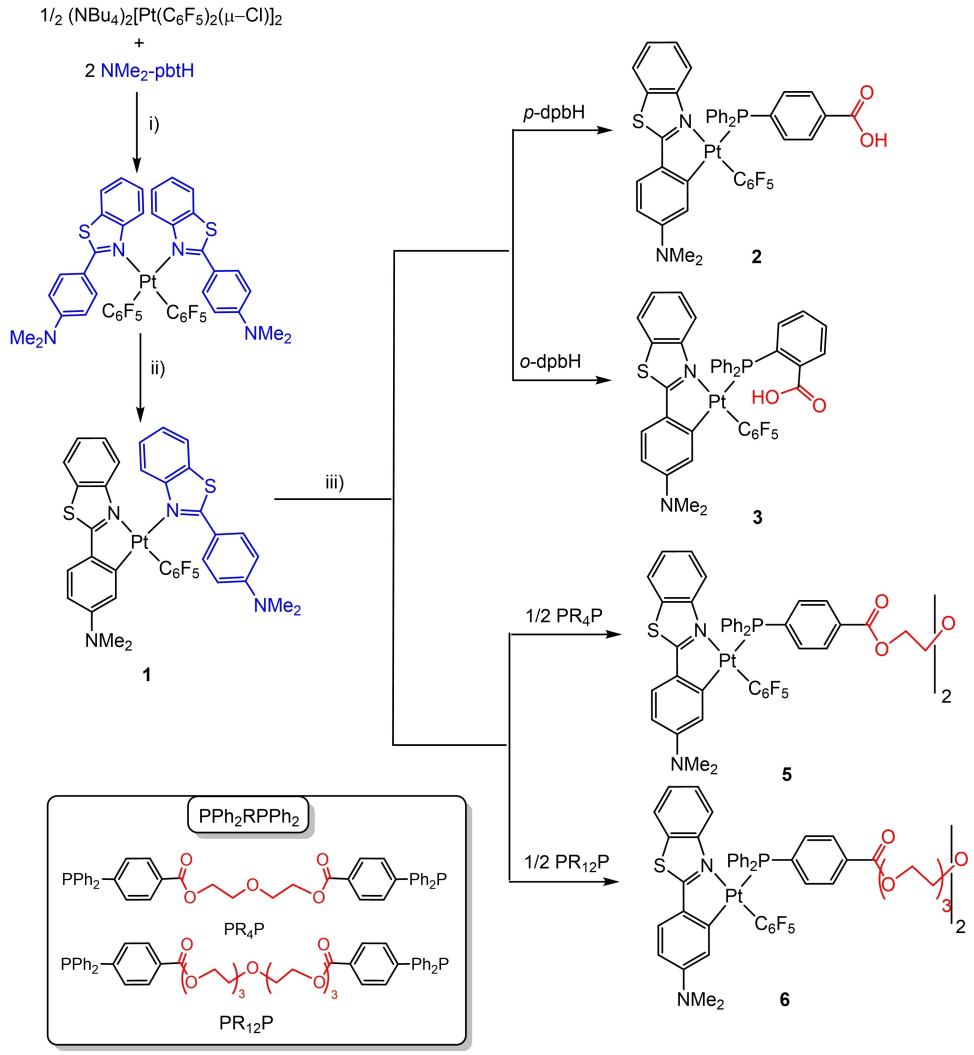

Scheme 1. Synthesis of **1**–**3**, **5** and **6**: i) $TlPF_6$, CH_2Cl_2, 298 K, 20 h; ii) toluene, Δ, 10 h; iii) CH_2Cl_2, 298 K, 10 h.

This complex is stable in [D_6]acetone but evolves slowly in warm [D_6]DMSO solution (38 °C, ~6 days) by a relatively easy OH activation and release of C_6F_5H as confirmed by $^{19}F\{^1H\}$ NMR (Figure S5). Monitoring of this evolution by $^{31}P\{^1H\}$ NMR (Figure S6) reveals that, in DMSO solvent, the signal due to **3** (δ 26.9; $^1J_{P-Pt}$ = 2056 Hz) is somewhat broad and also the presence of small amount of free *o*-dpbH (δ −5.7), that suggest the occurrence of a slow equilibrium between **3** and *o*-dpbH. After 38 h, **3** was still the major component, but the signal due to the deprotonated chelated complex [Pt(Me_2N-pbt)(*o*-dpb)] **4** (δ 8.8; $^1J_{P-Pt}$ = 4398 Hz) and oxidized phosphine (*o*-dpbHO, δ 28.8) are clearly visible. The signal of **4** gradually grows, while that of **3** decreases and after 62 h, and a new complex characterized by an AB system (δP_A 11.6, δP_B 21.1; $^2J P_A P_B$ = 438 Hz) [Pt(*o*-dpb)(C_6F_5)(*o*-dpbH)] **7** starts to be formed, being clearly visible upon 6 days. Although we have not detected any other P-containing species, the formation of the chelate complex **7**, is likely triggered by the N-opening of the hemilabile cyclometalated Me_2N-pbt group and coordination of free *o*-dpbH (Scheme 2). The N-opening of C^N ligand to give monocoordinated κ*C* ligand could be favored by the presence of free *o*-dpbH. Indeed, similar behavior has been observed in reactions of some *C,N*-cycloplatinated complexes in presence of excess of ligands.[27,32] Further protonation of the metalated C–Pt with simultaneous chelation of the phosphine and release of free ligand Me_2N-pbtH (observed by ^{1}H NMR) would give complex **7** (Scheme 2). Several attempts to obtain monocrystals of complex **3** evolve with formation of crystals of **7**, as has been confirmed by X-ray (Figure 1). Complex **4** is alternatively and straightforward formed by reaction of the dimer [{Pt(Me_2N-pbt)(μ-Cl)}$_2$] with 2 equiv. of *o*-dpbH in presence of Na_2CO_3 as base.

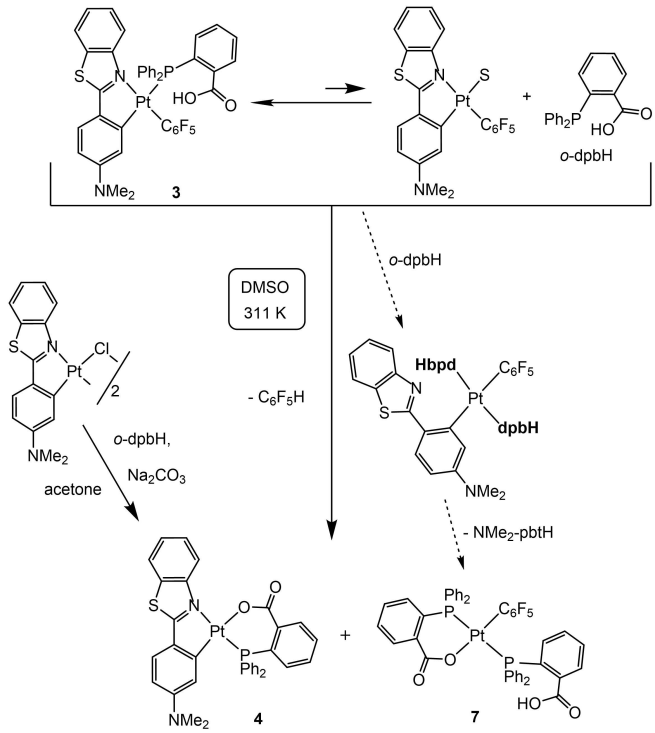

Scheme 2. Evolution of **3** in DMSO at 311 K.

The complexes were characterized by several conventional methods, including ESI-MS, ^{1}H, $^{31}P\{^1H\}$, $^{19}F\{^1H\}$ and $^{13}C\{^1H\}$ NMR spectroscopy, and CHN elemental analysis (Figures S1–S9). From the structural point of view, the most characteristic is the resonance due to the *ortho* proton ^{11}H, which appears as a doublet (**1**) or dd (**2**–**6**) with the expected Pt satellites ($^3J_{Pt-H}$ = 59–77 Hz), as the most shielded signal (δ 5.92–6.04) due to its proximity to the diamagnetic current of the *cis*-C_6F_5 ring. The $^{31}P\{^1H\}$ NMR spectra of **2**–**6** display a singlet in the range 23.4 to 26.9 ppm with $^1J_{P-Pt}$ values (1975–2056 Hz) characteristic of P *trans* to C. In complex **4**, the signal is notably up field (δ 8.81), due to the formation of a six membered cycle, and the $^1J_{P-Pt}$ coupling up to 4398 Hz, confirming the geometry of the chelating Ph_2P-COO^- ligand, which locates the P atom *trans* to the N atom of low *trans* influence.

The structures of complexes **2**, **4** and **7** were further confirmed by X-ray crystallography (Figure 1), and some crystallographic data are listed in Tables S1 and S2. All complexes display the expected slightly distorted square-planar geometry. The Pt–C, Pt–N, Pt–P and P–O bonding distances around the Pt are similar to those previously described.[27,33] In **2** and **4**, the Me_2N is essentially coplanar with the bt unit and with the Pt coordination plane, which favors π···π stacking in the crystal packing (Figure S10-S12). We note that crystals of **2**,

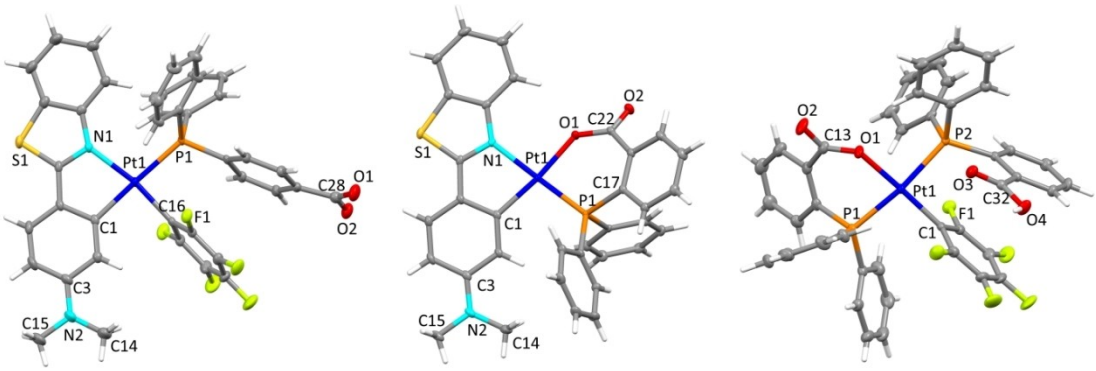

Figure 1. Molecular structures of **2**·*i*PrOH·CH_2Cl_2, **4**·$CHCl_3$ and **7**·2 MeOH (ellipsoids at 30% probability).

which were obtained by slow diffusion of *i*PrOH in a CH_2Cl_2 solution, crystallize as **2**·*i*PrOH·CH_2Cl_2. The *i*PrOH was incorporated through the formation of hydrogen bonds with the carboxylic acid of the *p*-dpbH (H···O1 = 2.025 Å, O2'···O = 2.566 Å), giving rise to the formation of dimers. Complex **7** crystallizes as **7**·2MeOH and the two molecules of MeOH are also involved in hydrogen bonding interactions. One is contacting with the CO group of the chelating Ph_2P-COO^- (O···H = 2.028 Å) ligand and the second with the hydroxy unit OH of the coordinated *o*-dpbH (O···H = 1.856 Å). As shown in Figure S12, further contacting through the MeOH of two distinct units (O···H = 1.948 Å) generates a cyclic dimer.

Photophysical properties and calculations

Absorption spectra. UV/Vis absorption of complexes **1**–**6** were collected in CH_2Cl_2 solutions (Table S3) and assignments were done from TD-DFT calculations in CH_2Cl_2 for selected complexes (**1**, **2** and **4**; Tables S4–S6 and Figures S13–S16). The electronic spectra, together with that of free ligand, are shown in Figure 2, whereas the comparison of the calculated (stick bars) and the experimental spectra for **1**, **2** and **4** are given in Figure S13. As shown in Figure 2, complex [Pt(Me_2N-pbt)(C_6F_5)(Me_2N-pbtH)] **1**, featuring the cyclometalated and the pending N-coordinated Me_2N-pbtH groups, displays a distinctive strong band at 395 nm and a shoulder 436 nm, respectively.

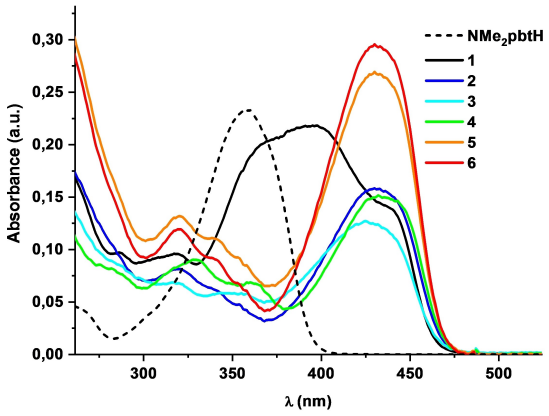

Figure 2. UV-vis absorption spectra of **L**, **1**–**6** in CH_2Cl_2 (5×10^{-5} M) at 298 K.

The low-energy shoulder, which coincides with the low energy band of the remaining cyclometalated complexes **2**–**6**, is assigned to a charge transfer transition ^{1}ILCT with a remarkable Me_2N to benzothiazole character on the cyclometalated group. In this complex, the most intense low energy absorption is S_2 (calcd 402 nm) and corresponds to the excitation HOMO→L + 1 located on the Me_2N-pbt. However, the strong band at 395 nm is contributed from two close excitations (S_3 and S_4; H-1→LUMO, L + 1) having mixed ^{1}IL'CT, located on the pending Me_2N-pbtH ligand (L'), and ^{1}L'LCT character. In the phosphine (**2**, **3**) and diphosphine (**5**, **6**) complexes, the low energy feature is mainly assigned, as in **1**, to a spin allowed charge-transfer (Me_2N →bt) transition located on the cyclometalated ligand, having in these complexes some ^{1}LL'CT contribution. The presence of two chromophores in the bimetallic complexes **5** and **6** is reflected in the strong difference in the intensity of this band, which essentially doubles its ε value (Figure 2, Table S3).

For complex **2**, the calculated two low energy absorptions correspond to HOMO→LUMO, L + 1 with the HOMO and L + 1 located on the Me_2N-pbt ligand and LUMO on the PhCOOH group (Figure 3). For the chelating complex **4**, the low energy band located at 435 nm has ^{1}ILCT character with negligible contribution of the PPh_2COO^- ligand because the increasing energy separation between the LUMO located on the Me_2N-pbt and the upper L + 1 having contribution of the $PCOO^-$ unit. The slight red shift of this band compared to that of complex **2** (430 nm) is reflected in the calculations (Figures 3 and S14–

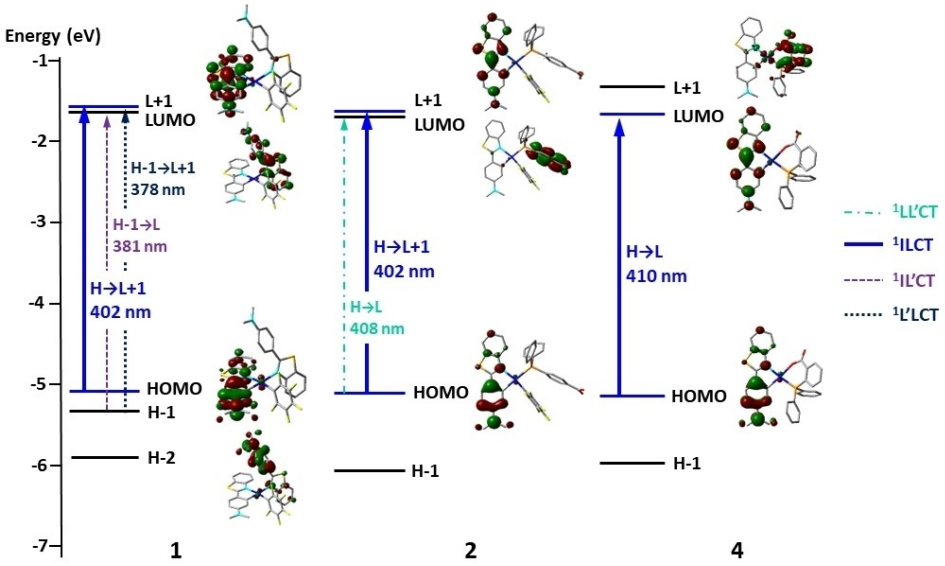

Figure 3. Schematic representation of selected frontier orbitals and the most important low energy absorption transitions of **1**, **2** and **4**.

S16). It is interesting to note that in these complexes the transitions having notable contribution from the platinum are located at higher energy. In complex **1**, the orbitals with remarkable Pt content (H-2 and H-3, close in energy) are involved in the excitations S_5 and S_7 located at 355 and 344 nm, having ^{1}ML'CT and ^{1}MLCT character, respectively. In complex **2**, the transition S_5 (H-2 to L+1) calculated at 334 nm has ^{1}MLCT character, whereas in complex **4**, are the excitations S_3 and S_4 (351, 347 nm), which present a mixed ^{1}MLCT/^{1}LL'CT parentage.

Table 1. Photophysical data of L and complexes **1**–**6** in different media (CH_2Cl_2 10^{-4} M or polystyrene 1:10 *w/w*).

Compound	Medium (T/K)	λ_{em}/nm (ϕ) [τ /μs]
Me_2N-pbtH	PS	426[a]
	CH_2Cl_2 (298)	418[a]
	CH_2Cl_2 (77)	421[a]
1	PS	490[vw], 560 (25%) [27.6]
	deg. CH_2Cl_2 (298)	474[vw], 562 [18.3]
	CH_2Cl_2 (298)	468[a], 555[w]
	CH_2Cl_2 (77)	458[vw], 552 [102]
2	PS	494[a], 568 (19%) [37.9]
	deg. CH_2Cl_2 (298)	478[a], 568 [35.4]
	CH_2Cl_2 (298)	476[a]
	CH_2Cl_2 (77)	466[w], 561 [165]
	DMSO (298)	490[a], 580
	PS	490[a], 564 (20%) [30.2]
	deg CH_2Cl_2 (298)	476[a], 568 [28.0]
	CH_2Cl_2 (298)	474[a]
	CH_2Cl_2 (77)	462[w], 557 [144]
4	PS	494[wa], 564 (17%) [32.3]
	deg. CH_2Cl_2 (298)	480[w], 564 [27.2]
	CH_2Cl_2 (298)	477[a]
	CH_2Cl_2 (77)	463[w], 562 [142]
5	PS	494[a], 568 (19%) [30.2]
	deg. CH_2Cl_2 (298)	484[a], 570 [18.1]
	CH_2Cl_2 (298)	482[a]
	CH_2Cl_2 (77)	468[w], 564 [154, 59%; 236, 41%]
6	PS	496[a], 570 (20%) [35.6]
	deg. CH_2Cl_2 (298)	484[a], 570 [22.6]
	CH_2Cl_2 (298)	483[a]
	CH_2Cl_2 (77)	472[w], 565 [133, 36%; 210, 64%]

[a] Lifetime lower than 4 ns. (deg: degassed).

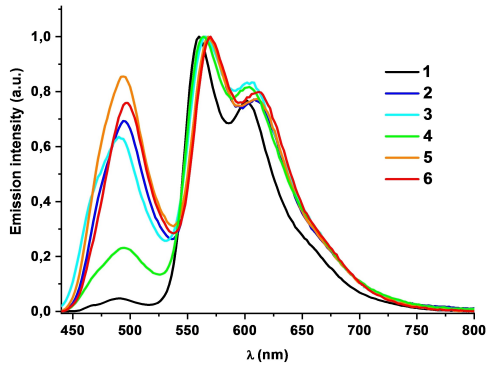

Figure 4. Emission spectra of **1**–**6** in PS 1:10 *w/w* at 298 K (λ_{ex} 420 nm).

Emission spectra. Table 1 summarizes the photophysical data of the complexes measured in CH_2Cl_2 solution (298, 77 K) and polystyrene (PS) film and selected spectra are provided in Figures 4–6. Remarkably, most complexes exhibit, upon excitation into the charge transfer intraligand band (λ_{ex} 420 nm), dual fluorescence and phosphorescence emissions that originate, according to calculations, from Pt-perturbed intraligand Me_2N

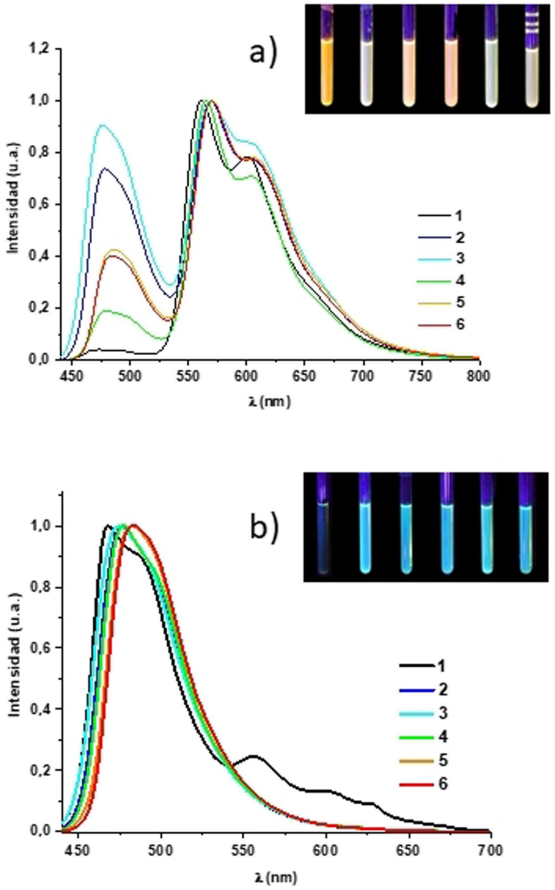

Figure 5. Emission spectra of **1**–**6** in CH_2Cl_2 (10^{-4} M) at 298 K (λ_{ex} 420 nm) a) degassed and b) aerated.

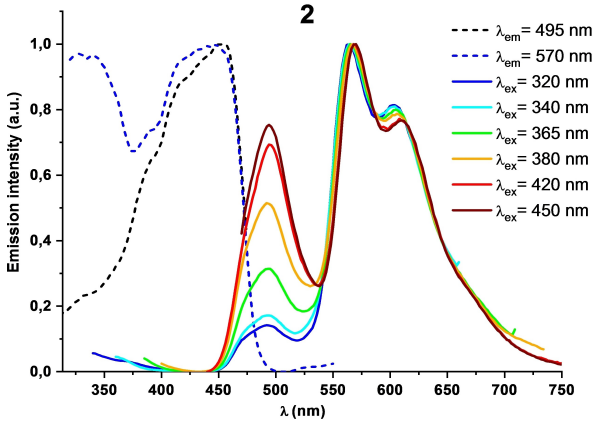

Figure 6. Excitation and emission spectra of **2** in polystyrene 1:10 *w/w* at 298 K.

-pbt charge transfer ^{1}ILCT and ^{3}ILCT, respectively. As can be seen in Figures 4 and 5, all phosphorus-based ligand complexes **2**–**6** display both in PS and in CH_2Cl_2 at 298 K a dual emission, which comprises a short-lived (< 4 ns) high energy unstructured band (HE) in the blue region (centered at ca. 490–496 nm in PS and 474–484 in CH_2Cl_2) and a long lived low well-structured energy band (LE) in the yellow-orange region (574–570 nm PS; 564–570 CH_2Cl_2). The most significant difference between fluid and doped systems is the slight bathochromic shift of the HE band in rigid PS (by ca. 10–14 nm).

As shown in Figure 5b, the short-lived HE band is essentially unaffected by the oxygen, being therefore ascribed to fluorescence (F) located on the Me_2N -pbt (^{1}ILCT). The emission lifetime of the LE band ranges between 30.2 and 37.9 μs in PS and from 18.1 to 35.4 μs in CH_2Cl_2 and is completely quenched in an air equilibrated CH_2Cl_2 solution, as shown in Figure 5b. These long-lived excited states and their strongly sensitivity to the presence of oxygen are indicative of triplet parentage. Interestingly, we observed that the ratio between both bands is excitation-dependent with a remarkable increase of the phosphorescent LE band by exciting at higher energies, as is illustrated for complex **2** in Figure 6, clearly evidencing hyper-intersystem crossing (HISC), that is, the occurrence of a distinctly faster population of the T_1 state from higher S_n states having notable metal contributions.[34] Our calculations suggest that for complex **2**, S_4 and S_5 excitations calculated at 345 and 333.8 nm, respectively (H-1, H-2→L + 1) have a notable platinum contribution (H-1 82% Pt; H-2 59% C^N, 37% Pt), whereas for complex **4** is S_4 having MLCT/L'LCT character (Table S6). In accordance with this behavior, the comparison of the excitation spectra of both bands reveals that while the fluorescent HE band mainly proceeds of excitation of the ^{1}ILCT, the phosphorescent LE band is also notably populated from high-energy excited states (below 350 nm; see Figure 6 for **2**). The presence of impurities was rigorously ruled out.

Based on TD-DFT calculations on complexes **2** and **4**, the spin density of the optimized T_1 state is primarily located on the Me_2Npbt with minor metal contribution (Figure 7). Therefore, the low energy band is ascribed to metal-perturbed intraligand phosphorescence ^{3}ILCT. Comparison of the energy maxima reveals a slight bathochromic shift for bimetallic complexes (**5**, **6** 484, 570 nm) and for the chelating *o*-dpb (**4** **480**, 564 nm) in relation to the related mononuclear complexes (**2** 478, 568 nm; **3** 476, 568 nm) and a minor blue shift in the fluorescence band by substituting the carboxyl unit from the *para* to the *ortho* position (**480** in **4** vs. 476 nm in **3**). This is indicative of the negligible role of the auxiliary ligands in the excited states in accordance with the calculations. The measured quantum yields, Φp, using a calibrated integrating sphere are similar in all complexes (17–20%).

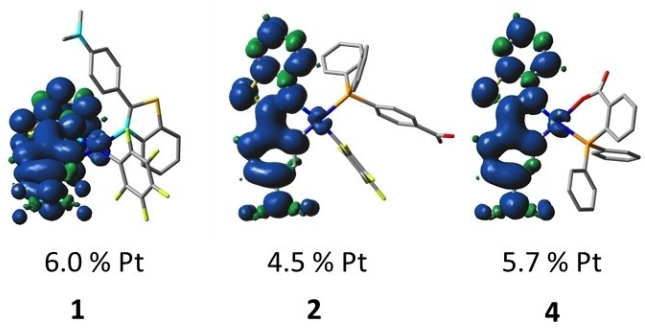

Figure 7. Spin-density distribution for the lowest triplet excited states in **1**, **2** and **4**.

It should be pointed out that dual emissions have been previously reported in some Pt, Ir and Au luminescent complexes, particularly featuring highly delocalized luminophores as ligands.[16b,28c,34–35] The growing interest in this type of phosphors might be attributed to its potential application, especially in the field of single component white-emitting diodes (WOLEDs).[34b,36] In these single white emitting molecules the emission can be fine-tuned from cold to warm white and its application in single component WOLEDs could avoid undesired phase separation and color variation problems that commonly occur in multiple-component emitters.[37] The behavior of complexes **2**–**6**, featuring Me_2N-pbt cyclometalating framework, indicates that they do not follow Kasha's rule, which states that emission from a luminophore will occur from the lowest lying excited state.[38] Dual F and P emissions in metal complexes is usually a consequence of the relatively slow rate of the $S_1 \rightarrow T_1$ intersystem crossing (ISC) due to the low contribution of the metal center in the involved π–π* ligand-centered excited state allowing the F ($S_1 \rightarrow S_0$) to compete with the ISC.[34a,39] In these systems, the rate constant for phosphorescence emission is also increased due to a proximal heavy atom. As suggested by DFT calculations on selected complexes **2** and **4**, the Pt contribution to the low-lying ILCT excitation is negligible (Figure S17). Consequently, the intersystem crossing (κ_{ICS}) from the S_1 to the emitting T_1 state decreases, being slow enough to allow the effective population of both S_1 and T_1 states and leading to the observed dual emission.

In fluid solution, the lower ratio F/P is observed for the chelating complex **4**, increasing the F in the order **4** < **6** ~ **5** < **2** < **3**, which is reflected in the final color of the emission (Figure 5a), nearly warm-white for complexes **2**, **5** and **6**. The ratio F/P decreases for all complexes in rigid media, both in PS and in glassy CH_2Cl_2 solution at 77 K, with the lower F/P value for the most constrained compound **4** featuring two chelating ligands (Figures 4 and S18). In contrast to the behavior of complexes **2**–**6**, the precursor complex **1**, bearing the pendant N-coordinated Me_2N-pbtH ligand, is only weakly fluorescent in strictly degassed CH_2Cl_2 and in PS (< 5%), but phosphoresces at 560 nm with a quantum yield of 25% in PS. Interestingly, in air-equilibrated CH_2Cl_2, the phosphorescent emission diminishes notably in **1** and is completely lost in complexes **2**–**6** while the fluorescence remains, leading to a weak final naked-eye blue emission (Figure 5b). For **1**, the lower *trans* influence of the N-pyridine donor atom in relation to P for complexes **2**–**6**, likely causes a shortening in the Pt–C metalated bond, rendering the ISC more efficient. In addition, our calculation indicates that whereas in complexes **2** and **4** the T_2 state is well above of the T_1 (and also the S_1), in complex **1**, the T_2 having IL'CT character is close to T_1 (T_1 2.2754 eV; T_2 2.4871 eV) and below to low lying

excitations $S_{1\text{-}4}$, (considering vertical transitions), thus decreasing the $\Delta E(S_1-T_2)$ gap (Figure 8), which has been previously suggested to increase the Intersystem Crossing. Therefore, in complex **1**, an ISC from S_1 to T_2 followed by a fast internal conversion from T_2 to T_1 could also efficiently populate the lowest triplet state at a faster rate than for the phosphorous containing complexes **2**–**6**.

DFT calculations for the three complexes **1**, **2** and **4** demonstrated that the vertical $\Delta E(T_1\text{-}S_0)$ (2.01273 **1**; 1.98693 **2**; 1.99012 eV **4**) is above the energy necessary to activate ground-state molecular oxygen ($^3O_2$, 0.98 eV) and promote the formation of $^1O_2$ species.[40] This fact and the long lifetime of the phosphorescence band for these complexes (Table 1) could explain the observed quenching of the metal-perturbed ^{3}ILCT by the oxygen molecular $^3O_2$.[41] To asses if these complexes are able to generate singlet oxygen, the triplet $^3O_2$ emission was monitored for complexes **2** and **4** in CH_2Cl_2 solution (10^{-2} M). As shown in Figures 9 and S19, both complexes display an intense emission band at around 1270 nm upon excitation at 455 nm. The value of the quantum yield (Φ_Δ) of **4** in MeCN solution, determined by the changes in the absorption spectra of the $^1O_2$ scavenger, 1,3-diphenylbenzofuran in the presence of **4** and in the presence of $[Ru(bpy)_3]Cl_2$, as the reference (see the Supporting Information, Experimental Section and Figure S20), was calculated to be 34%. This result indicates that these complexes might be used as photosensitizers to provide cytotoxic $^1O_2$ in photodynamic therapy.

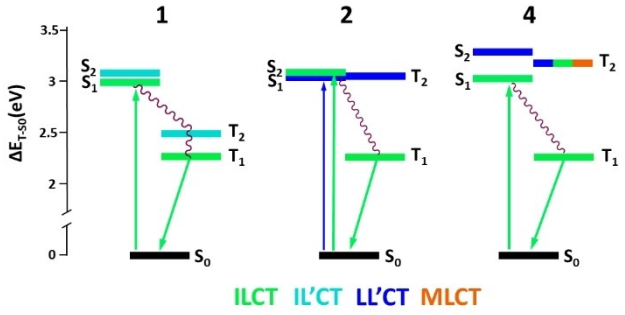

Figure 8. Schematic representation of the energy levels of selected singlet and triplet states calculated for the ground state geometry of **1**, **2** and **4**.

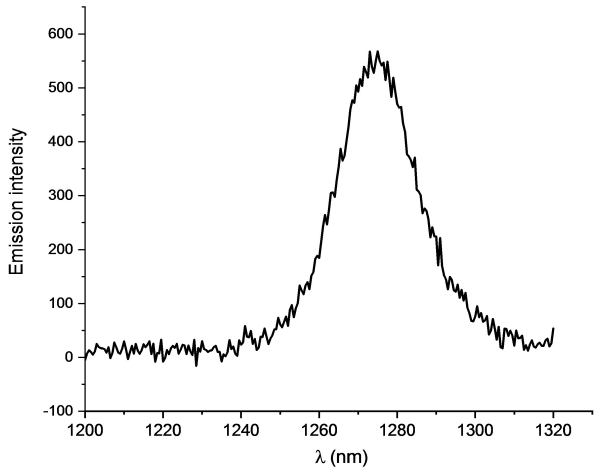

Figure 9. Emission band of the singlet oxygen from a fresh solution of **4** in CH_2Cl_2 (10^{-2} M).

In anticipation of photo-biological studies on these complexes (see below), we also examined the emission of the complexes in *aerated* DMSO. Under these conditions, the phosphorescence was completely quenched for complexes **2**–**6**. Interestingly, for these complexes, we observed that, in aerated DMSO solutions, upon prolonged exciting at 365 nm with a hand UV-Vis lamp (1 min), the initial blue emission, due to the ^{1}ILCT fluorescence, was gradually changing from the bottom appearing initially a white warm and finally a pale orange enhanced emission. The intense orange emission was switched off by simply shaking of the solution and the process can be repeatedly again by exposure to the UV-Vis light. This behavior, attributed to a photoinduction of the metal perturbed ^{3}ILCT phosphorescence, was not observed in solvents others than DMSO (CH_2Cl_2, $CHCl_3$, THF, acetone or MeOH). This phenomenon, although unusual has some precedents.[42] Thus, Che et al. reported an enhancement of the phosphorescent emission of a cycloplatinated complex upon prolonged exposure to light in DMSO[42a] and Lu et al, more recently published that the long-lived phosphorescence of Au^I arylacetylide complexes could be reversibly activated in aerated DMSO by photo-irradiation.[42b] It was proposed that during the photo-activation process, trace amounts of DMSO molecules were oxidized by sensitized singlet oxygen into dimethylsulfone ($DMSO_2$), creating a local free $^3O_2$ microenvironment that triggers the quenched phosphorescence molecular.

Complex **2** was chosen for a more detailed study and the results are depicted in Figure 10. Figure 10a shows the photographs of the emission of a freshly prepared solution of complex **2** (non-degassed DMSO, 10^{-4} M) upon photoirradiation at λ_{ex} 365 nm for 5 min. Shaking the solution in air extinguishes the orange emission and return to the blue emission (see the Supporting Movie). The emission spectra were recorded on the spectrofluorometer upon excitation at 365 nm for 17 min. As can be seen in Figure 10b,c, in addition to the fluorescence band at 488 nm, an structured emission band with a peak maximum at 588 nm gradually developed, after a short incubation period of about 30s, increasing very fast during the first 7 min and then more slowly reaching the maximum at about 17 min. Concomitantly, the F band at 488 nm only experiences a minor decreasing of intensity of about 10%. The intensities of both bands with the time and excitation spectra are depicted in Figure 10b,c, while the change in the color rendering index is indicated by the *xy* coordinates on a chromaticity diagram (Commission International de l'Eclairage, CIE) in Figure 10d. The excitation spectrum monitoring the 580 nm band resembles to that of monitoring at 488 nm, but develops a peak at ~330 nm, indicating also hyper-intersystem crossing (HISC) in this solvent. Thus, phosphorescent emission not only derives from the ^{1}ILCT but also emanates from high energy excited states having ^{1}ILCT/^{1}MLCT character.

Upon shaking the solution to allow oxygenation of the solution, the phosphorescence is quenched, and the initial

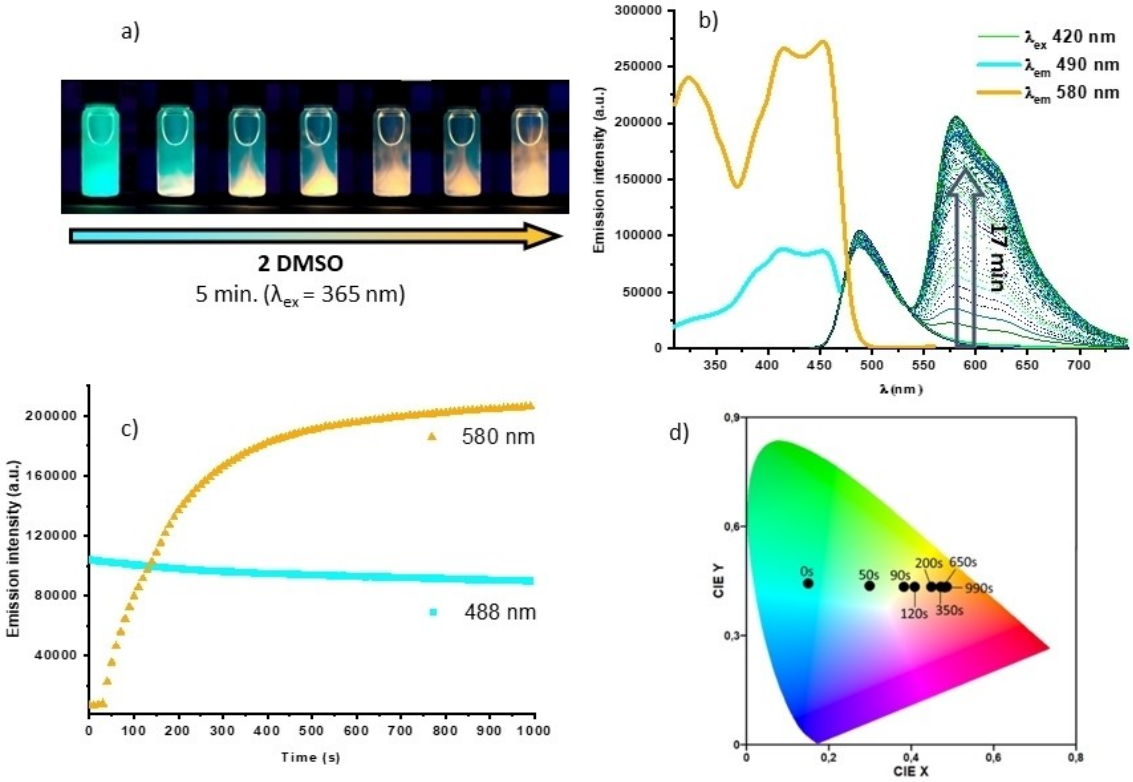

Figure 10. a) Evolution of **2** in DMSO with irradiation at λ_{ex} 365 nm. b) Excitation and emission of **2** in DMSO 10^{-4} M in the presence of O_2 with different irradiation times. c) Intensity of the emission maxima vs. time, d) CIE color coordinates of the emission.

blueish emission is restored. This photoswitched-*on* and oxygen-quenched-*off* cycle of the phosphorescent band process can be repeated at least five times with similar intensities on both bands. As was previously noted, the role of DMSO solvent is decisive. In aerated conditions, the ^{3}ILCT excite state is deactivated by energy transfer to $^3O_2$ to produce singlet $^1O_2$ (Figure S19b). As noted before, it has been reported that this behavior is likely driven through the photooxidation of two molecules of DMSO by each sensitized $^1O_2$ to produce dimethylsulfone, thus causing a local deoxygenation that activates the phosphorescence. In our system, ^{19}F, and ^{31}P NMR monitoring reveals that complex **2** is relatively photostable. However, upon prolonged irradiation of a DMSO solution of **2** with a hand-held lamp at 365 nm, we were unable to detect the generation of dimethylsulfone by ^{1}H NMR. Therefore, we suspect that the amount of $DMSO_2$ generated seems to be to free the microenvironment of **2** from O_2 but not to be detected by ^{1}H NMR.

Biological studies

We next analyzed several biological capabilities of the ligand Me_2N-pbtH and complexes **1**–**6**. As noted before, in DMSO solution complex **1** evolves to the solvate [Pt(pbt)(C_6F_5)(DMSO)],[30] whereas complex **3** evolves to the bischelating **4**, as was assessed by NMR spectroscopy. In DMSO/cellular medium the dinuclear derivative **5** precipitates to a large extend, whereas complexes **2** and **6** were found to be stable with no evidence of relevant changes by UV-Vis spectroscopy (Figure S21). For all complexes was determined their cytotoxicity against two different tumor and one non-tumor cell lines by the MTS-based method, their relative lipophilicity by RP-UPLC (Reversed-phase chromatography) and the interaction with DNA by gel electrophoresis. In addition, their cellular location and a possible mechanism of action by depolymerization of tubulin were studied by confocal microscopy and immuno-staining, respectively. Furthermore, considering the easy generation of singlet oxygen from these derivatives and their possible capabilities as photosensitizers, the cytotoxicity in the presence and absence of UV light irradiation was measured for one of the non-cytotoxic compounds.

Cytotoxic activity: The IC_{50} values were determined against human tumor: A549 (lung carcinoma) and HeLa (cervix carcinoma) and nontumor 184B5 (breast epithelium) cell lines after cellular exposure to the compounds for 72 h and compared to cisplatin as a reference (Table 2 and Figure S22). The ligand Me_2N-pbtH and complexes **1**, **4** and **5** did not show cytotoxic effects against A549 cells, probably due to the lack of free carboxylic groups, and in case of **5** could be additionally due to its low solubility in aqueous solutions. Thus, they were considered non-toxic, and not further analyzed in HeLa and 184B5 cells. The lack of toxicity of **1** contrasts with the moderate toxicity previously found in the related 2-phenyl-

Table 2. IC_{50} values [μM][a] and selectivity index[b] of the cytotoxic complexes **2**, **3** and **6** in human cell lines A549, HeLa and 184B5, compared with cisplatin.

Complex	IC_{50}[a] A549	HeLa	184B5	SI[b] A549	HeLa
2	8.39 ± 0.75	38.82 ± 1.05	23.46 ± 0.46	2.80	0.60
3	11.59 ± 1.40	16.51 ± 0.57	18.60 ± 1.63	1.60	1.13
6	10.43 ± 0.05	43.25 ± 1.23	NT (> 100)	> 9.5	> 2.3
cisplatin	6.45 ± 0.47[c]	13.60 ± 0.99[d]	5.73 ± 0.45	0.89	0.42

[a] IC_{50} values are presented as mean ± standard error of the mean of three different experiments performed in sextuplicate. [b] As determined in ref. [29]. [c] As determined in ref. [30]. [d] As determined in ref. [27]. NT: nontoxic; IC_{50} values could not be determined as a relevant percentage of cytotoxicity was not achieved at any concentration tested.

benzothiazole-DMSO complex [Pt(pbt)(C_6F_5)(DMSO)].[30] In contrast, **2**, **3** and **6** exhibited cytotoxic activity in both tumor cell lines, in all cases with values of IC_{50} lower in A549 cells.

Compound **2** displayed the lowest IC_{50} value towards the A549 cell line (8.39 μM), being almost as cytotoxic as cisplatin, and **6** the highest in HeLa cell line (43.25 μM). All three complexes were more active towards the A549 cell line than to HeLa, in accordance with previous results found with related [Pt(C^N)(C_6F_5)L] complexes (C^N = ppy, dfppy, L = DMSO, *p*-dpbH).[29] Interestingly, higher IC_{50} values towards breast 184B5 nontumor cells were observed by **3** (18.60 μM) and **6** (> 100 μM, considered nontoxic). IC_{50} value of complex **2** towards this cell line (23.46 μM) although was also higher towards A549 cells, was lower towards HeLa. Of note, IC_{50} values towards 184B5 cells showed by cisplatin (5.73 μM) was the lowest of all complexes tested (Table 2). In agreement, similar IC_{50} values for cisplatin toward these cells were previously reported.[43]

Based on the IC_{50} assessment, the higher values of selectivity index (SI; > 2) were demonstrated by cytotoxic compound **6** towards tumor A549 (> 9.5) and HeLa (> 2.3) cells, and to a lower extent by complex **2** towards A549 cells (2.80) against nontumor 184B5 cells. SI values for complex **3** were 1.60 (A549) and 1.13 (HeLa), which indicated low selective toxicity towards cancer cells, since SI < 2 is assumed to give general toxicity.[44] The lowest SI values (< 1) were shown by complex **2** in HeLa (0.60) and by cisplatin (0.89 in A549 and 0.42 in HeLa). Low SI values for cisplatin, related platinum derivatives, and other organometallic complexes with cytotoxic activities toward A549, HeLa, and other cancer cell lines have been previously described, although not using 184B5 cells as nontumor cell lines[29,45]

Relative lipophilicity: In order to stablish a possible correlation between the cytotoxicity and lipophilicity, the relative hydrophobicity of **1**–**6** was determined by RP-UPLC. Complexes were dissolved in methanol/H_2O (10% *v/v*, ~10 μm) and mobile phase used were A (H_2O with 0.1% HCOOH) and B (acetonitrile with 0.1% HCOOH). The relative lipophilicity of the complexes was based on the retention times (t_R) accounting the relative interaction between the hydrophilic mobile phase and hydrophobic stationary phase (Aquity UPCL BEH C_{18}). The more lipophilic complexes should have longer t_R.[46] As was expected, the mononuclear complexes give lower retention times than the diplatinum complexes (complex/t_R min **1**/6.0; **4**/6.3; **2**/7.8; **3**/7.9 vs. **5**/11.8; **6**/10.4, 11.6). Intriguingly, two different retention peaks, with identical isotopic mass, were found for complex **6**. This fact might be tentatively due to the very long carbon chain of the diphosphane ($PR_{12}P$) that induces the displacement along the column of two conformers. The RP-UPLC was interfaced with an QTOF mass spectrometer using ESI(+). The ESI-MS of the 5.98 min of **1** shows the isotopic pattern at *m/z* 616.05, assigned to the loss of Hpbt ligand ($[M-\text{Hpbt}]^+$, whereas the isotopic pattern for the rest of samples (**2**–**6**) in their retention time corresponds to the $[M+H]^+$ peak (Figure S23). There is no a clear relationship between the lipophilicity and cytotoxicity. Indeed, the low lipophilic **2** and **3** revealed the highest cytotoxicity in A549 and HeLa cells, respectively. However, the most lipophilic **5** is not cytotoxic and **6**, of high lipophilicity, exhibited the lowest cytotoxicity in HeLa cells and was not cytotoxic towards breast 184B5 nontumor cells.

*Photoinduced cytotoxicity of complex **4***: Luminescent cyclometalated Ir^{III} and also Pt^{II} compounds have been previously described as efficient photosensitizers for the generation of singlet oxygen ($^1O_2$),[22a] and a few of them were reported to exhibit photodynamic therapeutic effects.[22a,c,47] As the complexes reported here are able to generate $^1O_2$ upon irradiation, they can be considered as potential tools in phototheranostics. We decided to evaluate the potential use of complex **4** in photodynamic therapy based on its fast cellular internalization (see below) and non-cytotoxic effects in normal cell culture conditions. Its photostability was initially monitored by NMR analysis under similar irradiation conditions and using prolonged exposures times. To assess its photobiological activity, A549 and HeLa cells were treated with complex **4** in Hank's balanced salt solution (HBSS) for 1 h at 37 °C to give the compound time to enter the cells. Subsequently, the cells were irradiated with a 396 nm LED lamp located 91 mm apart (~ 5 mW/cm^2) for 1 min ("photoinduced" plate). After irradiation, the cells were washed and incubated in complete RPMI medium (without complex **4**) for another 72 h. Then, the viability of the cells (IC_{50}) was assessed by the MTS test, as described in the Experimental Section. As shown in Figure 11, upon light irradiation for 1 min, complex **4** exhibited high antitumor activity in both cell lines, leading to IC_{50} values of 0.83 and 1.50 μM in A549 and HeLa cells, respectively. Notably, the induced phototoxicity lead to higher anticancer activity than that determined for **2**, **3** and **6** cytotoxic compounds and cisplatin under non-irradiated conditions (Table 2). Increasing radiation time of A549 cells up to 3 min barely increased cytotoxicity, achieving an IC_{50} value of 0.63 μM. Non-irradiated cells did not show cytotoxicity of **4** in any of the cell lines (Figure 11). Additional tests irradiating cells up to 30 min in HBSS alone further discarded direct phototoxic effects of UV light.

The relevant photoinduced cytotoxicity found with complex **4** using UV light with a wavelength close to its strong low energy ^{1}ILCT electronic absorption (Figure 2) and a very short period of time (1 min) is remarkable, since previously reported transition metal complexes that have entered clinical studies for cancer photodynamic therapy required much longer photo-

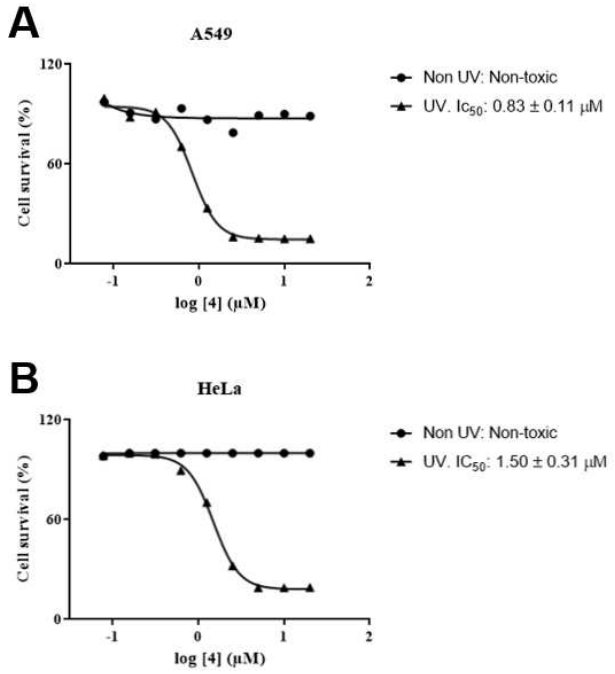

Figure 11. Dose–response curves for a) A549 and B) HeLa cells treated with complex **4**, either with (triangles) or without (circles) UV light: irradiation with a UV 396 nm LED for 1 min and the MTS cytotoxic assay performed after 72 h. Non-UV, non-irradiated cells were manipulated identically to irradiated. IC_{50} values are presented as mean ± standard error of the mean of three different experiments performed in sextuplicate.

induced exposures. Thus, the Ru^{II} derivative TLD1433, which is in phase clinical study for treating invasive bladder cancer, required photoinduction exposures of 48 minutes or longer to reach IC_{50} values of 0.062 μM (SKMEL28 melanoma cell line, 400–700 nm; 34.7 mW/cm^2).[48] In case of WST11, a Pd derivative already used in trials for prostate cancer photodynamic therapy,[49] when tested in H5 V endothelial cells rendered an IC_{50} value of 0.8 μM after 10 min of irradiation (650–800 nm, 12 J/cm^2).[50] Given that these results depend on each particular experimental set up, to make a clear comparison of their photoinduced cytotoxic potency it would require measurements under the same conditions. Potential applications of Pt^{II} compounds in photodynamic therapy were also explored.[22a] In this way, analyses of the photophysical properties of a Pt^{II}-BODIPY derivative revealed that it was able to enhance the cytotoxic $^1O_2$ production.[40] Furthermore, a cyclometalated Pt^{II} complex was reported to induce irreversible DNA single strand breaks following irradiation, and that oxygen was essential for the photoinduced action.[22c] Based on its optical and biological properties, we could also hypothesize that upon irradiation of cells in presence of **4**, the metal perturbed ^{3}ILCT excited state of the complex is able to promote intracellular generation of cytotoxic $^1O_2$ by energy transfer to the molecular oxygen, to generate reactive oxygen species, the main mechanism for photodynamic therapy-initiated cell death.[48] Overall, it is clear that complex **4** is a non-cytotoxic 2-(4-dimethylaminophenyl) benzothiazole based cycloplatinated complex that rapidly penetrates and accumulates in the cytoplasm of cells (see later) and can act as an effective photosensitizer in cancer cell lines. Altogether, these properties highlight its potential for photodynamic therapy applications against tumors.

Interaction of complexes with DNA: Most platinum-containing molecules exert cytotoxic effects by binding to DNA through various mechanisms, and depending on the ancillary ligands, they can either covalently bind nitrogenous bases or act as DNA intercalators or aggregators.[10a–d,51] In order to evaluate their capacity to interact with DNA complexes **1** (non-cytotoxic as a reference), **2** and **6** (both cytotoxic) were incubated in increasing molar ratios with a fixed amount of pBR322 plasmid DNA. Complex **3** (cytotoxic) was not assessed due to its chemical instability. To provide a basis for comparison, cisplatin was used under the same concentrations and conditions. Finally, the ability of complexes and cisplatin to modify the electrophoretic mobility of the plasmid forms was assessed in agarose gels as previously described[52] (Figure S24). Binding of cisplatin to plasmid DNA results in an electrophoretic shift, decreasing the mobility of the CCC (covalently closed circular, supercoiled) plasmid form and increasing the mobility of the OC (open circular, relaxed; Figure S24, left).[29,52] Conversely, no electrophoretic mobility changes were observed after DNA treatment with any of the complexes tested (**1**, **2** and **6**) in the same conditions (Figure S24, right). These results suggest that these compounds do not interact with the DNA, therefore pointing to an alternative cytotoxic mechanism of action for **2** and **6**.

Lack of DNA binding properties in different types of cycloplatinated platinum(II) derivatives have been previously reported by others,[52–53] and also by us, in similar complexes ([Pt(C^N)(C_6F_5)L] [C N = C-deprotonated 2-phenylpyridine, 2-(2,4-difluorophenylpyridine); L = $PPh_2C_6H_4COOH$, $PPh_2C_6H_4CONHCH_2COOMe$, $P(C_6H_4SO_3Na)$][29] containing biocompatible phosphines as ancillary ligands. Of note, a progressive reduction of both the CCC and OC bands staining intensity was noticed after treatment with complex **1**, and to a lesser extend with **6** (Figure S24), an effect that was intensified in a concentration-dependent manner but neither exhibited by **2** nor by cisplatin. Possible interpretations of these results could be a complex-mediated induction of either DNA precipitation or DNA degradation.

Effects on microtubule polymerization: Given our previous experience with related cycloplatinated complexes[27,29] and the lack of effect on DNA interaction of the 2-(4-dimethylaminophenyl)benzothiazole based cycloplatinated complexes, we decided to test whether cytotoxic compounds **2** and **6** were able to inhibit tubulin polymerization as a mechanism of toxicity. A549 cells were exposed to 100 μM **2** and **6** for 6 h or 100 μM nocodazole for 2 h. Cells were fixed and stained for tubulin with an appropriate antibody as described in the Experimental Section. The captured laser-scanning confocal microscopy (LSCM) images are shown in Figure 12. As expected, treatment with the microtubule targeting agent nocodazole profoundly altered microtubule dynamics in A549 cells, causing a notable microtubule disassembly. On the contrary, A549 cell exposed to compounds **2** and **6** did not show any sign of tubulin depolymerization even though some of them started to

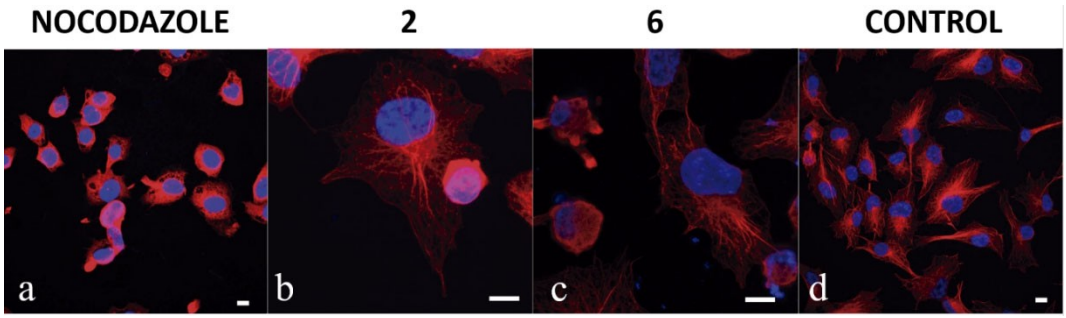

Figure 12. Laser scanning confocal microscopy images of fixed A549 cells treated with a) 100 μM nocodazole (microtubule targeting agent) for 2 h, b) 100 μM compound **2** for 6 h, or c) 100 μM compound **6** for 6 h; d) control cells. Red: tubulin antibody staining (λ_{ex} 543 nm); Blue: nuclei marker (DAPI, λ_{ex} 405 nm). CONTROL, untreated cells (scale bars: 10 μm).

show detachment from the substrate and blebbing, which is a sign of toxicity and potential cell death.

Thus, these results suggest that depolymerization of tubulin is not involved in the cytotoxicity mechanism of compounds **2** and **6**, and contrast with our previous findings on related cycloplatinated systems based on ppy, dfppy and pbt chromophores that showed different levels of microtubule disassembling capacity.[27,29] As we have neither found evidence of interaction with DNA nor altering tubulin polymerization in case of **2** and **6**, alternative mechanisms should be considered to explain their cytotoxic activity.

Cytolocalization: In order to study the cellular uptake of the ligand (Me_2N-pbtH) and the cycloplatinated complexes **1**, **2**, **4**–**6**, a confocal fluorescence imaging study was carried out in lung mouse embryonic fibroblasts (LMEFs) and A549 cells at 37 °C, in a 5% CO_2 atmosphere, as described in the Experimental Section. We did not observe any intracellular fluorescence signal in cells without compounds even after incubation for 24 h. As shown in Figure 13, addition of the ligand and compounds **1**, **2**, **4**, **6**, elicited a visible intracellular green fluorescence signal, indicating successful internalization. Interestingly, none of the compounds were found inside the nucleus of the cells, which is in agreement with our DNA interaction assays. In accordance with its lack of toxicity, compound **5** did not enter the cells (data not shown), probably due to its low solubility in the medium.

Time-course analysis to monitor their internalization was performed into A549 cells. Ten μM solutions were added to the cells and micrographs were captured at the indicated times (Figure 13). Surprisingly, Me_2N -pbtH was found to internalize very quickly as revealed by the bright green fluorescence within the first 2–5 min (Figure 13). Compound **1** was found to enter the cells faster than the rest of the compounds, while **2** and **6** were slower and peaked at 22 h.

However, although **1** entered the cells very fast, total cellular accumulation was higher for **2**, **4** and **6** (Figure 13), what is also in agreement with the antiproliferative action of **2** and **4** and the negligible cytotoxicity found for complex **1**. All of

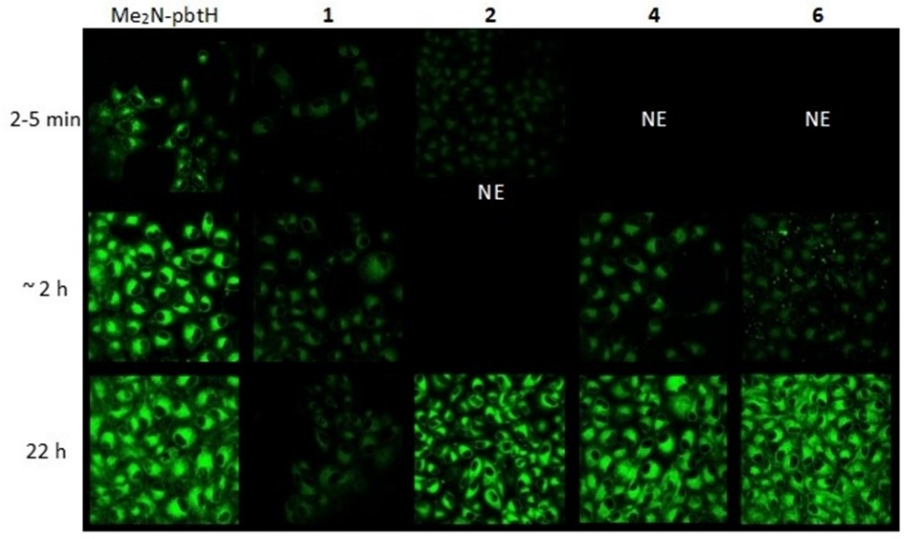

Figure 13. Laser scanning confocal microscopy images of live A549 cells incubated with 10 μM Me_2N-pbtH (ligand), **1**, **2**, **4** or **6** for the indicated times (λ_{ex} 405 nm. NE: non-emissive).

them showed the same pattern of cellular staining along the incubation time, displaying a predominant emission in the perinuclear region of the cells. To identify the preferred localization within the cytoplasm staining assays with specific intracellular organelle biotrackers for mitochondria (MitoTracker®) and lysosomes (Lysotracker®) were performed in combination with the free ligand Me_2N -pbtH and complexes **1** and **2**. Figure 14 shows LMEFS treated for 22 h with 10 μM ligand, **1** or **2**, and the MitoTracker® and Lysotracker® markers. Compounds **1**, **2**, **4** and **6**, as well as the ligand (Me_2N -pbtH), showed lack of accumulation in mitochondria and minor accumulation in the endosomal/lysosomal compartments (Figures 14 and S25, respectively). Similar results were observed in A549 tumor cells, although with less detail due to their smaller proportion of cytoplasm and roundish morphology.

Given that the observed perinuclear localization of the compounds in the cells (Figure 13) was suggestive of Golgi apparatus localization, we incubated the cells with the commercially available Golgi apparatus marker BODIPY TR C5 Ceramide BSA and Me_2N -pbtH or compound **2**. As shown in Figure 15, at concentration 10 μM, the emission of the compounds is seen in green (a) and the Golgi marker in red (b), a clear coincidence is observed when they are superimposed (c). This indicates that most of the signal colocalized with the Golgi apparatus marker, pointing that our compounds localized preferentially in this organelle. These photos have been taken after 2 h of exposure to the ligand (and the marker) and 4 h with compound **2**.

For the platinum compound **2**, which is slower to internalize in the cell, this distribution does not change much with the time. However, for the ligand, when this is added before the marker, it enters so rapidly that it ceases to fully colocalize in the Golgi apparatus and begins to be observed in scattered lysosomes.

In this context, by taking advantage of their favorable luminescence properties, a growing number of d^6 (Ir^{III}, Ru^{II}) and d^8 (Pt^{II}, Au^{III}) cyclometalated complexes, have been successfully developed exhibiting selective organelle staining with specific organelle accumulation.[2d,5a,9a,b,d,e,14b–d,15,21a,54] Among subcellular organelles (mitochondria, nucleus, lysosomes, ER, Golgi apparatus), Golgi apparatus targeting metal complexes are extremely rare,[5a,21a,55] despite this organelle is a key structure for transporting and secreting some important proteins/enzymes, such as cyclooxygenase-2, which are overexpressed in cancer cells. To date, a few Ir^{III} cyclometalated complexes have reported specific target to Golgi apparatus.[5a,21a] Lo and co-workers reported some dendritic cationic luminescent $[\{Ir(N\hat{}C)_2\}_n(bpy\text{-}n)](PF_6)_n$ complexes exhibiting a high cytotoxicity (HeLa line), which was suggested to originate primarily from their binding to the Golgi body.[56] By contrast, Wong, Ho and co-workers have reported a negligible cytotoxic neutral heteroleptic $[Ir(C\hat{}N)_2(C\hat{}N')]$ complex, based on the donor-acceptor Me_2N-PhPy and Ar_2B-PhPy cyclometalated groups, that demonstrated

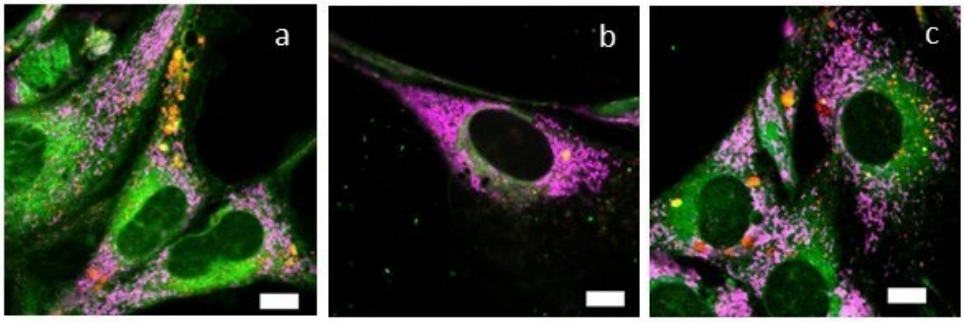

Figure 14. Laser scanning confocal microscopy images of live LMEF cells incubated with 10 μM a) Me_2N-pbtH, b) **1** or c) **2** for 22 h and simultaneous co-staining with LysoTracker and MitoTracker. Green: Ligand/compound (λ_{ex} 405 nm); Red: LysoTracker (Lysosomal marker, λ_{ex} 543 nm); Magenta: MitoTracker (Mitochondrial marker, λ_{ex} 633 nm). Yellow indicates colocalization between ligand or compounds (green) and LysoTracker (red). There is no evidence of co-localization of ligand or compound with MitoTracker (scale bars: 10 μm).

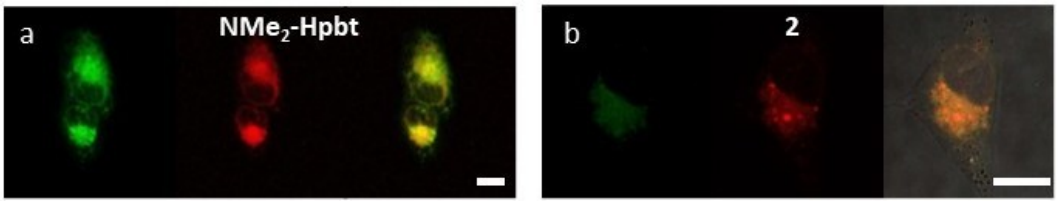

Figure 15. Laser scanning confocal microscopy images of live A549 cells incubated with a) 10 μM Me_2N-pbtH (ligand) for 2 h or b) 10 μM **2** for 4 h (ligand/compound signal in green, λ_{ex} 405 nm, left) and in the presence of BODIPY TR C5 ceramide (Golgi apparatus marker; signal in red, λ_{ex} 543 nm, center). Superimposed images are shown on the right; yellow/orange indicates colocalization between ligand/compound and BODIPY TR C5 ceramide in the Golgi apparatus (scale bars: 10 μm).

a strong two-photon induced phosphorescence with specific Golgi-imaging in HeLa and A549 cell lines.[57]

Here, we show that Me_2N-pbtH ligand and **2** localize in the Golgi complex. However, the ligand has not demonstrated to be cytotoxic on human tumoral cells, rapidly accumulates in living cells and mainly localizes in the Golgi bodies demonstrating an emission intensity even higher than that of the commercial Golgi marker itself. These results are of great interest, demonstrating a possible application of the Me_2N-pbtH ligand as a marker ("tracker") of the Golgi apparatus organelle.

Conclusions

By using the donor–acceptor 2-(4-dimethylaminophenyl) benzothiazole ligand (Me_2N -pbtH), novel neutral pentafluorophenyl mono- and dinuclear cycloplatinated complexes featuring biologically active phosphine donors as auxiliary ligands (**1**–**3**, **5**, **6**) have been prepared. Complex [Pt(Me_2N -pbt)(C_6F_5)(*o*-dpbH)] **3** is unstable in DMSO giving rise to [Pt(Me_2N -pbt)(*o*-dpbH)] **4** and small amounts of [Pt(*o*-dpb)(C_6F_5)(*o*-dpbH)] **7**. Complexes **1**–**6** emit both fluorescence and metal-perturbed, intraligand-based phosphoresce caused by slow intersystem crossing (ISC; S_1 to T_1). Due to the hyper-ISC phenomenon, the ratio between both bands is excitation-dependent giving rise to nearly warm-white emissions for complexes **2**, **5** and **6**. Moreover, they exhibit intriguing photoinduced phosphorescent enhancement emission in non-degassed DMSO, ascribed to local oxidation of DMSO to $DMSO_2$ by sensitized $^1O_2$ singlet, which remove $^3O_2$, as demonstrated in complex **2**.

There is continuing search for new biocompatible photosensitizers for use in photodynamic therapy. In this context, these complexes are able to generate singlet-oxygen species with potential in photodynamic therapy. In vitro studies reveal that only **2**, **3** and **6** are active against A549 and HeLa cancer cell lines, with higher efficiency in A549. Interestingly, complex **6** is highly selective for tumor cells without causing any cytotoxic effect on the nontumor cell line. The lipophilicity of the bimetallic complexes featuring ethylene glycol units (**5** and **6**) is higher than the mononuclear derivatives (**1**–**5**), but no clear relationship with the antitumoral activity was found. However, we demonstrated that under a short photoirradiation time (1 min) complex **4** exhibits high cytotoxicity with IC_{50} values at nanomolar concentration in both type of tumor cell line, which has relevance for those engaged in PDT research. These complexes do not enter the nucleus and do not interfere with tubulin depolymerization, as previously observed in related cycloplatinated systems based on ppy, dfppy, and pbt chromophores. Cytolocalization studies revealed that ligand Me_2N-pbtH and these complexes enter the cells and accumulate preferentially in the Golgi apparatus, subsequently transferring to the endosomal/lysosomal compartment. Importantly, the non-cytotoxic Me_2N -pbtH ligand could be used as an alternative or new cheap Golgi marker. Consequently, given their different cytotoxic profiles these complexes can be used as subcellular organelle markers or cytotoxic compounds either in their parent form or after photoactivation.

Deposition Numbers 2081196 (for **2**·*i*PrOH·CH_2Cl_2), 2081197 (for **4**·$CHCl_3$) and 2081198 (for **7**·2MeOH) contain the supplementary crystallographic data for this paper. These data are provided free of charge by the joint Cambridge Crystallographic Data Centre and Fachinformationszentrum Karlsruhe Access Structures service.

Acknowledgements

This work was supported by the Spanish Ministerio de Ciencia e Innovación (Project PID2019-109742GB–I00), the European Regional Development Fund, the ADER (Gobierno de La Rioja; Project 2017-I–IDD-00031) and the Fundación Rioja Salud (Gobierno de La Rioja). I.M.L. was supported by a Miguel Servet contract (CP15/00198 and CP20/00029) from the Instituto de Salud Carlos III-FEDER (Fondo Europeo de Desarrollo Regional, a way to build Europe) and European Social fund (ESF) "Investing in your future". R. L., G.M. and E.A.-A. are grateful to UR and to the Spanish Association Against Cancer (AECC), respectively, for their PhD grants.

Conflict of Interest

The authors declare no conflict of interest.

Keywords: cell imaging · cyclometallation · dual emission · platinum · photocytotoxicity

[1] B. Rosenberg, L. Vancamp, J. E. Trosko, V. H. Mansour, *Nature* **1969**, *222*, 385.
[2] a) M. Fanelli, M. Formica, V. Fusi, L. Giorgi, M. Micheloni, P. Paoli, *Coord. Chem. Rev.* **2016**, *310*, 41–79; b) V. Brabec, O. Hrabina, J. Kasparkova, *Coord. Chem. Rev.* **2017**, *351*, 2–31; c) B. J. Pages, K. B. Garbutcheon-Singh, J. R. Aldrich-Wright, *Eur. J. Inorg. Chem.* **2017**, 1613–1624; d) R. G. Kenny, C. J. Marmion, *Chem. Rev.* **2019**, *119*, 1058–1137; e) P. Štarha, J. Vančo, Z. Trávníček, *Coord. Chem. Rev.* **2019**, *380*, 103–135; f) T. C. Johnstone, K. Suntharalingam, S. J. Lippard, *Chem. Rev.* **2016**, *116*, 3436–3486; g) J. D. White, M. M. Haley, V. J. DeRose, *Acc. Chem. Res.* **2016**, *49*, 56–66; h) X. Wang, X. Wang, Z. Guo, *Acc. Chem. Res.* **2015**, *48*, 2622–2631; i) S. Medici, M. Peana, V. M. Nurchi, J. I. Lachowicz, G. Crisponi, M. A. Zoroddu, *Coord. Chem. Rev.* **2015**, *284*, 329–350; j) W. Liu, R. Gust, *Coord. Chem. Rev.* **2016**, *329*, 191–213; k) K. M. Deo, D. L. Ang, B. McGhie, A. Rajamanickam, A. Dhiman, A. Khoury, J. Holland, A. Bjelosevic, B. Pages, C. Gordon, J. R. Aldrich-Wright, *Coord. Chem. Rev.* **2018**, *375*, 148–163.
[3] R. Oun, Y. E. Moussa, N. J. Wheate, *Dalton Trans.* **2018**, *47*, 6645–6653.
[4] a) A. Jain, *Coord. Chem. Rev.* **2019**, *401*, 213067; b) V. Brabec, J. Kasparkova, V. Menon, N. P. Farrell in *Metallo-Drugs: Development and Action of Anticancer Agents Vol. 18*, De Gruyter, Berlín, **2018**, Chapter 12; c) N. P. Farrell, *Chem. Soc. Rev.* **2015**, *44*, 8773–8785.
[5] a) C. Caporale, M. Massi, *Coord. Chem. Rev.* **2018**, *363*, 71–91; b) N. Mirzadeh, T. S. Reddy, S. K. Bhargava, *Coord. Chem. Rev.* **2019**, *388*, 343–359; c) E. B. Bauer, A. A. Haase, R. M. Reich, D. C. Crans, F. E. Kühn, *Coord. Chem. Rev.* **2019**, *393*, 79–117; d) B. Bertrand, M. R. M. Williams, M. Bochmann, *Chem. Eur. J.* **2018**, *24*, 11840–11851; e) V. Fernández-Moreira, M. C. Gimeno, *Chem. Eur. J.* **2018**, *24*, 3345–3353.
[6] a) X. Wang, Z. Guo, *Chem. Soc. Rev.* **2013**, *42*, 202–224; b) J. S. Butler, P. J. Sadler, *Curr. Opin. Chem. Biol.* **2013**, *17*, 175–188; c) D. Gibson, *J. Inorg. Biochem.* **2019**, *191*, 77–84; d) E. Andrea, *Curr. Med. Chem.* **2019**, *26*, 694–728.

[7] a) M. Imran, W. Ayub, I. S. Butler, F. Zia-ur-Rehman, *Coord. Chem. Rev.* **2018**, *376*, 405–429; b) J. B. Patrick, S. M. Fiona, J. S. Peter, *Anti-Cancer Agents Med. Chem.* **2007**, *7*, 75–93.

[8] a) Đ. Miodragović, E. P. Swindell, Z. Sattar Waxali, A. Bogachkov, T. V. O'Halloran, *Inorg. Chim. Acta* **2019**, *496*, 119030; b) K. H. Son, J. H. Hong, J. W. Lee, *Int. J. Nanomed.* **2016**, *11*, 5163–5185; c) R. J. Browning, P. J. T. Reardon, M. Parhizkar, R. B. Pedley, M. Edirisinghe, J. C. Knowles, E. Stride, *ACS Nano* **2017**, *11*, 8560–8578; d) J. P. Parker, Z. Ude, C. J. Marmion, *Metallomics* **2016**, *8*, 43–60.

[9] a) M. Mauro, A. Aliprandi, D. Septiadi, N. S. Kehr, L. De Cola, *Chem. Soc. Rev.* **2014**, *43*, 4144–4166; b) K. K.-W. Lo, S. P.-Y. Li, *RSC Adv.* **2014**, *4*, 10560–10585; c) K. K. W. Lo, A. W. T. Choi, W. H. T. Law, *Dalton Trans.* **2012**, *41*, 6021–6047; d) Q. Zhao, C. Huang, F. Li, *Chem. Soc. Rev.* **2011**, *40*, 2508–2524; e) E. Baggaley, J. A. Weinstein, J. A. G. Williams, *Coord. Chem. Rev.* **2012**, *256*, 1762–1785.

[10] a) J. Suryadi, U. Bierbach, *Chem. Eur. J.* **2012**, *18*, 12926–12934; b) H.-K. Liu, P. J. Sadler, *Acc. Chem. Res.* **2011**, *44*, 349–359; c) T. Zou, J. Liu, C. T. Lum, C. Ma, R. C.-T. Chan, C.-N. Lok, W.-M. Kwok, C.-M. Che, *Angew. Chem. Int. Ed.* **2014**, *53*, 10119–10123; *Angew. Chem.* **2014**, *126*, 10283–10287; d) J. Ruiz, C. Vicente, C. de Haro, A. Espinosa, *Inorg. Chem.* **2011**, *50*, 2151–2158; e) L. Rao, T. K. West, G. Saluta, G. L. Kucera, U. Bierbach, *Chem. Res. Toxicol.* **2010**, *23*, 1148–1150; f) J. P. Parker, M. Devocelle, M. P. Morgan, C. J. Marmion, *Dalton Trans.* **2016**, *45*, 13038–13041.

[11] a) H. Xiao, R. Qi, T. Li, S. G. Awuah, Y. Zheng, W. Wei, X. Kang, H. Song, Y. Wang, Y. Yu, M. A. Bird, X. Jing, M. B. Yaffe, M. J. Birrer, P. P. Ghoroghchian, *J. Am. Chem. Soc.* **2017**, *139*, 3033–3044; b) A. A. Hostetter, M. F. Osborn, V. J. DeRose, *ACS Chem. Biol.* **2012**, *7*, 218–225; c) R. W.-Y. Sun, A. L.-F. Chow, X.-H. Li, J. J. Yan, S. Sin-Yin Chui, C.-M. Che, *Chem. Sci.* **2011**, *2*, 728–736.

[12] a) M. Ravera, E. Gabano, M. J. McGlinchey, D. Osella, *Inorg. Chim. Acta* **2019**, *492*, 32–47; b) Y. Guo, Y. He, S. Wu, S. Zhang, D. Song, Z. Zhu, Z. Guo, X. Wang, *Inorg. Chem.* **2019**, *58*, 13150–13160; c) H. Chen, F. Chen, W. Hu, S. Gou, *J. Inorg. Biochem.* **2018**, *180*, 119–128.

[13] G. Darren, P. P. James, J. M. Celine, *Anti-Cancer Agents Med. Chem.* **2010**, *10*, 354–370.

[14] a) D.-L. Ma, H.-Z. He, K.-H. Leung, D. S.-H. Chan, C.-H. Leung, *Angew. Chem. Int. Ed.* **2013**, *52*, 7666–7682; *Angew. Chem.* **2013**, *125*, 7820–7837; b) K. Y. Zhang, Q. Yu, H. Wei, S. Liu, Q. Zhao, W. Huang, *Chem. Rev.* **2018**, *118*, 1770–1839; c) K. K.-W. Lo, K. K.-S. Tso, *Inorg. Chem. Front.* **2015**, *2*, 510–524; d) Y. You, *Curr. Opin. Chem. Biol.* **2013**, *17*, 699–707; e) Y. Chen, R. Guan, C. Zhang, J. Huang, L. Ji, H. Chao, *Coord. Chem. Rev.* **2016**, *310*, 16–40; f) C. Huang, T. Li, J. Liang, H. Huang, P. Zhang, S. Banerjee, *Coord. Chem. Rev.* **2020**, *408*, 213178; g) R. Guan, L. Xie, T. W. Rees, L. Ji, H. Chao, *J. Inorg. Biochem.* **2020**, *204*, 110985.

[15] K. Li, G. S. Ming Tong, Q. Wan, G. Cheng, W.-Y. Tong, W.-H. Ang, W.-L. Kwong, C.-M. Che, *Chem. Sci.* **2016**, *7*, 1653–1673.

[16] a) V. W.-W. Yam, V. K.-M. Au, S. Y.-L. Leung, *Chem. Rev.* **2015**, *115*, 7589–7728; b) E. V. Puttock, M. T. Walden, J. A. G. Williams, *Coord. Chem. Rev.* **2018**, *367*, 127–162; c) M. Yoshida, M. Kato, *Coord. Chem. Rev.* **2018**, *355*, 101–115; d) A. Aliprandi, D. Genovese, M. Mauro, L. D. Cola, *Chem. Lett.* **2015**, *44*, 1152–1169; e) H. B. Gray, S. Záliš, A. Vlček, *Coord. Chem. Rev.* **2017**, *345*, 297–317.

[17] a) A. Haque, L. Xu, R. A. Al-Balushi, M. K. Al-Suti, R. Ilmi, Z. Guo, M. S. Khan, W.-Y. Wong, P. R. Raithby, *Chem. Soc. Rev.* **2019**, *48*, 5547–5563; b) M. Yoshida, M. Kato, *Coord. Chem. Rev.* **2020**, *408*, 213194; c) J. Herberger, R. F. Winter, *Coord. Chem. Rev.* **2019**, *400*, 213048.

[18] a) N. Cutillas, G. S. Yellol, C. de Haro, C. Vicente, V. Rodríguez, J. Ruiz, *Coord. Chem. Rev.* **2013**, *257*, 2784–2797; b) I. Omae, *Coord. Chem. Rev.* **2014**, *280*, 84–95; c) A. Zamora, S. A. Pérez, V. Rodríguez, C. Janiak, G. S. Yellol, J. Ruiz, *J. Med. Chem.* **2015**, *58*, 1320–1336; d) S. Jürgens, F. E. Kühn, A. Casini, *Curr. Med. Chem.* **2018**, *25*, 437–461; e) M. Vaquero, N. Busto, N. Fernández-Pampín, G. Espino, B. García, *Inorg. Chem.* **2020**, *59*, 4961–4971; f) S. Garbe, M. Krause, A. Klimpel, I. Neundorf, P. Lippmann, I. Ott, D. Brünink, C. A. Strassert, N. L. Doltsinis, A. Klein, *Organometallics* **2020**, *39*, 746–756.

[19] a) K. Suntharalingam, A. Łęczkowska, M. A. Furrer, Y. Wu, M. K. Kuimova, B. Therrien, A. J. P. White, R. Vilar, *Chem. Eur. J.* **2012**, *18*, 16277–16282; b) D.-L. Ma, C.-M. Che, S.-C. Yan, *J. Am. Chem. Soc.* **2009**, *131*, 1835–1846.

[20] A. I. Solomatina, P. S. Chelushkin, T. O. Abakumova, V. A. Zhemkov, M. Kim, I. Bezprozvanny, V. V. Gurzhiy, A. S. Melnikov, Y. A. Anufrikov, I. O. Koshevoy, S.-H. Su, P.-T. Chou, S. P. Tunik, *Inorg. Chem.* **2019**, *58*, 204–217.

[21] a) K. Qiu, Y. Chen, T. W. Rees, L. Ji, H. Chao, *Coord. Chem. Rev.* **2019**, *378*, 66–86; b) A. Bergamo, P. J. Dyson, G. Sava, *Coord. Chem. Rev.* **2018**, *360*, 17–33.

[22] a) D. Ashen-Garry, M. Selke, *Photochem. Photobiol.* **2014**, *90*, 257–274; b) T. Chatzisideri, S. Thysiadis, S. Katsamakas, P. Dalezis, I. Sigala, T. Lazarides, E. Nikolakaki, D. Trafalis, O. A. Gederaas, M. Lindgren, V. Sarli, *Eur. J. Med. Chem.* **2017**, *141*, 221–231; c) R. E. Doherty, I. V. Sazanovich, L. K. McKenzie, A. S. Stasheuski, R. Coyle, E. Baggaley, S. Bottomley, J. A. Weinstein, H. E. Bryant, *Sci. Rep.* **2016**, *6*, 22668; d) P. I. Djurovich, D. Murphy, M. E. Thompson, B. Hernandez, R. Gao, P. L. Hunt, M. Selke, *Dalton Trans.* **2007**, 3763–3770.

[23] a) N. H. Nam, P. T. Dung, P. T. Thuong, *Med. Chem.* **2011**, *7*, 127–134; b) M. Singh, S. K. Singh, *Anti-Cancer Agents Med. Chem.* **2014**, *14*, 127–146; c) R. S. Keri, M. R. Patil, S. A. Patil, S. Budagumpi, *Eur. J. Med. Chem.* **2015**, *89*, 207–251; d) L. Hroch, L. Aitken, O. Benek, M. Dolezal, K. Kuca, F. Gunn-Moore, K. Musilek, *Curr. Med. Chem.* **2015**, *22*, 730–747; e) A. A. Weekes, A. D. Westwell, *Curr. Med. Chem.* **2009**, *16*, 2430–2440.

[24] a) A. K. Sharma, J. W. Schultz, J. T. Prior, N. P. Rath, L. M. Mirica, *Inorg. Chem.* **2017**, *56*, 13801–13814; b) J. Jia, M. Cui, J. Dai, B. Liu, *Dalton Trans.* **2015**, *44*, 6406–6415; c) K. Serdons, C. Terwinghe, P. Vermaelen, K. Van Laere, H. Kung, L. Mortelmans, G. Bormans, A. Verbruggen, *J. Med. Chem.* **2009**, *52*, 1428–1437.

[25] a) N. Amdursky, Y. Erez, D. Huppert, *Acc. Chem. Res.* **2012**, *45*, 1548–1557; b) C. Linus, R. J. Michael, L. F. Cara, S. Tim, *Curr. Top. Med. Chem.* **2012**, *12*, 122–144; c) F. Hualong, C. Mengchao, *Curr. Med. Chem.* **2018**, *25*, 2736–2759.

[26] a) Y.-P. Zeng, C.-W. Gao, L.-J. Hu, H.-H. Chen, G.-Y. Chen, G.-N. Li, Z.-G. Niu, *Acta Chim. Slov.* **2015**, *62*, 6; b) Y.-J. Yuan, Z.-T. Yu, H.-L. Gao, Z.-G. Zou, C. Zheng, W. Huang, *Chem. Eur. J.* **2013**, *19*, 6340–6349; c) X. Xu, X. Yang, Y. Wu, G. Zhou, C. Wu, W.-Y. Wong, *Chem. Asian J.* **2015**, *10*, 252–262; d) Y.-J. Yuan, J.-Y. Zhang, Z.-T. Yu, J.-Y. Feng, W.-J. Luo, J.-H. Ye, Z.-G. Zou, *Inorg. Chem.* **2012**, *51*, 4123–4133.

[27] E. Lalinde, M. T. Moreno, R. Lara, I. P. López, E. Alfaro-Arnedo, J. G. Pichel, S. Piñeiro-Hermida, *Chem. Eur. J.* **2018**, *24*, 2440–2456.

[28] a) R. Lara, E. Lalinde, M. T. Moreno, *Dalton Trans.* **2017**, *46*, 4628–4641; b) N. Giménez, R. Lara, M. T. Moreno, E. Lalinde, *Chem. Eur. J.* **2017**, *23*, 5758–5771; c) N. Giménez, E. Lalinde, R. Lara, M. T. Moreno, *Chem. Eur. J.* **2019**, *25*, 5514–5526.

[29] G. Millán, N. Giménez, R. Lara, J. R. Berenguer, M. T. Moreno, E. Lalinde, E. Alfaro-Arnedo, I. P. López, S. Piñeiro-Hermida, J. G. Pichel, *Inorg. Chem.* **2019**, *58*, 1657–1673.

[30] J. R. Berenguer, J. G. Pichel, N. Giménez, E. Lalinde, M. T. Moreno, S. Piñeiro-Hermida, *Dalton Trans.* **2015**, *44*, 18839–18855.

[31] L. K. Batchelor, E. Păunescu, M. Soudani, R. Scopelliti, P. J. Dyson, *Inorg. Chem.* **2017**, *56*, 9617–9633.

[32] a) V. Sicilia, S. Fuertes, A. Martín, A. Palacios, *Organometallics* **2013**, *32*, 4092–4102; b) A. R. Esmaeilbeig, M. G. Haghighi, S. Nikahd, S. Hashemi, M. Mosarezaee, M. Rashidi, S. M. Nabavizadeh, *J. Organomet. Chem.* **2014**, *755*, 93–100.

[33] B. Zhang, L. Zhang, C. Liu, Y. Zhu, M. Tang, C. Du, M. Song, *Dalton Trans.* **2014**, *43*, 7704–7707.

[34] a) F. Geist, A. Jackel, R. F. Winter, *Inorg. Chem.* **2015**, *54*, 10946–10957; b) M. Bachmann, O. Blacque, K. Venkatesan, *Chem. Eur. J.* **2017**, *23*, 9451–9456.

[35] a) M. Z. Shafikov, D. N. Kozhevnikov, M. Bodensteiner, F. Brandl, R. Czerwieniec, *Inorg. Chem.* **2016**, *55*, 7457–7466; b) S. Kumar, Y. Hisamatsu, Y. Tamaki, O. Ishitani, S. Aoki, *Inorg. Chem.* **2016**, *55*, 3829–3843; c) A. J. Howarth, D. L. Davies, F. Lelj, M. O. Wolf, B. O. Patrick, *Inorg. Chem.* **2014**, *53*, 11882–11889; d) A. Belyaev, I. Kolesnikov, A. S. Melnikov, V. V. Gurzhiy, S. P. Tunik, I. O. Koshevoy, *New J. Chem.* **2019**, *43*, 13741–13750.

[36] a) Q. Wang, D. Ma, J. Ding, L. Wang, Q. Qiao, H. Jia, B. E. Gnade, J. Hoshikawa-Halbert, *Org. Electron.* **2015**, *19*, 157–162; b) C. Duan, C. Han, R. Du, Y. Wei, H. Xu, *Adv. Opt. Mater.* **2018**, *6*, 1800437; c) M. Bachmann, D. Suter, O. Blacque, K. Venkatesan, *Inorg. Chem.* **2016**, *55*, 4733–4745; d) S. Reineke, M. Thomschke, B. Lüssem, K. Leo, *Rev. Mod. Phys.* **2013**, *85*, 1245–1293; e) X. Yang, Z. Wang, S. Madakuni, J. Li, G. E. Jabbour, *Adv. Mater.* **2008**, *20*, 2405–2409; f) H. Yang, J. Zheng, S.-K. Peng, X.-W. Zhu, M.-Y. Wan, W. Lu, D. Li, *Chem. Commun.* **2019**, *55*, 4635–4638; g) H. Liu, F. Liu, P. Lu, *J. Mater. Chem. C* **2020**, *8*, 5636–5661.

[37] V. Adamovich, J. Brooks, A. Tamayo, A. M. Alexander, P. I. Djurovich, B. W. D'Andrade, C. Adachi, S. R. Forrest, M. E. Thompson, *New J. Chem.* **2002**, *26*, 1171–1178.

[38] M. Kasha, *Discuss. Faraday Soc.* **1950**, *9*, 14–19.

[39] P. Irmler, F. S. Gogesch, C. B. Larsen, O. S. Wenger, R. F. Winter, *Dalton Trans.* **2019**, *48*, 1171–1174.
[40] F. Ponte, M. E. Alberto, B. C. De Simone, N. Russo, E. Sicilia, *Inorg. Chem.* **2019**, *58*, 9882–9889.
[41] E. Wolcan, *Inorg. Chim. Acta* **2020**, *509*, 119650.
[42] a) S. C. F. Kui, F.-F. Hung, S.-L. Lai, M.-Y. Yuen, C.-C. Kwok, K.-H. Low, S. S.-Y. Chui, C.-M. Che, *Chem. Eur. J.* **2012**, *18*, 96–109; b) S. Wan, W. Lu, *Angew. Chem. Int. Ed.* **2017**, *56*, 1784–1788; *Angew. Chem.* **2017**, *129*, 1810–1814; c) S. Wan, J. Lin, H. Su, J. Dai, W. Lu, *Chem. Commun.* **2018**, *54*, 3907–3910.
[43] S. Assinder, J. Street, S. Fraser, *J. Cancer Sci. Ther.* **2015**, https://doi.org/10.4172/1948-5956.S1.041_033.
[44] a) R. B. Badisa, S. F. Darling-Reed, P. Joseph, J. S. Cooperwood, L. M. Latinwo, C. B. Goodman, *Anticancer Res.* **2009**, *29*, 2993–2996; b) J. A. Valderrama, V. Delgado, S. Sepúlveda, J. Benites, C. Theoduloz, P. Buc Calderon, G. G. Muccioli, *Molecules* **2016**, *21*, 1420–3049.
[45] a) C. Li, K.-W. Ip, W.-L. Man, D. Song, M.-L. He, S.-M. Yiu, T.-C. Lau, G. Zhu, *Chem. Sci.* **2017**, *8*, 6865–6870; b) E. Petruzzella, R. Sirota, I. Solazzo, V. Gandin, D. Gibson, *Chem. Sci.* **2018**, *9*, 4299–4307; c) P. W. Prasetyaningrum, A. Bahtiar, H. Hayun, *Sci. Pharm.* **2018**, *86*, 25–37; d) N. Pantelić, B. B. Zmejkovski, D. D. Marković, J. M. Vujić, T. P. Stanojković, T. J. Sabo, G. N. Kaluđerović, *Metals* **2016**, *6*, 2075–4701.
[46] J. Yellol, S. A. Pérez, A. Buceta, G. Yellol, A. Donaire, P. Szumlas, P. J. Bednarski, G. Makhloufi, C. Janiak, A. Espinosa, J. Ruiz, *J. Med. Chem.* **2015**, *58*, 7310–7327.
[47] a) C. Wang, L. Lystrom, H. Yin, M. Hetu, S. Kilina, S. A. McFarland, W. Sun, *Dalton Trans.* **2016**, *45*, 16366–16378; b) J. Pracharova, G. Vigueras, V. Novohradsky, N. Cutillas, C. Janiak, H. Kostrhunova, J. Kasparkova, J. Ruiz, V. Brabec, *Chem. Eur. J.* **2018**, *24*, 4607–4619; c) L. C.-C. Lee, A. W.-Y. Tsang, H.-W. Liu, K. K.-W. Lo, *Inorg. Chem.* **2020**, *59*, 14796–14806; d) A. Ionescu, R. Caligiuri, N. Godbert, L. Ricciardi, M. La Deda, M. Ghedini, N. Ferri, M. G. Lupo, G. Facchetti, I. Rimoldi, I. Aiello, *Appl. Organomet. Chem.* **2020**, *34*, e5455.
[48] S. Monro, K. L. Colón, H. Yin, J. Roque, P. Konda, S. Gujar, R. P. Thummel, L. Lilge, C. G. Cameron, S. A. McFarland, *Chem. Rev.* **2019**, *119*, 797–828.
[49] I. S. Gill, A.-R. Azzouzi, M. Emberton, J. A. Coleman, E. Coeytaux, A. Scherz, P. T. Scardino, *J. Urol.* **2018**, *200*, 786–793.
[50] A. Brandis, O. Mazor, E. Neumark, V. Rosenbach-Belkin, Y. Salomon, A. Scherz, *Photochem. Photobiol.* **2005**, *81*, 983–993.
[51] a) J. C. Dabrowiak, *Metals in medicine*, John Wiley and Sons Ltd., Chichester, UK, **2009**, ch 4, p. 109; b) J. K. Muenzner, T. Rehm, B. Biersack, A. Casini, I. A. M. de Graaf, P. Worawutputtapong, A. Noor, R. Kempe, V. Brabec, J. Kasparkova, R. Schobert, *J. Med. Chem.* **2015**, *58*, 6283–6292; c) Y. Zhang, Q. Luo, W. Zheng, Z. Wang, Y. Lin, E. Zhang, S. Lü, J. Xiang, Y. Zhao, F. Wang, *Inorg. Chem. Front.* **2018**, *5*, 413–424.
[52] M. Frik, J. Jimenez, V. Vasilevski, M. Carreira, A. de Almeida, E. Gascon, F. Benoit, M. Sanau, A. Casini, M. Contel, *Inorg. Chem. Front.* **2014**, *1*, 231–241.
[53] M. Frik, J. Fernández-Gallardo, O. Gonzalo, V. Mangas-Sanjuan, M. González-Alvarez, A. Serrano del Valle, C. Hu, I. González-Alvarez, M. Bermejo, I. Marzo, M. Contel, *J. Med. Chem.* **2015**, *58*, 5825–5841.
[54] a) F. L. Thorp-Greenwood, R. G. Balasingham, M. P. Coogan, *J. Organomet. Chem.* **2012**, *714*, 12–21; b) A. Zamora, G. Vigueras, V. Rodríguez, M. D. Santana, J. Ruiz, *Coord. Chem. Rev.* **2018**, *360*, 34–76.
[55] K. K.-W. Lo, *Acc. Chem. Res.* **2015**, *48*, 2985–2995.
[56] K. Y. Zhang, H.-W. Liu, T. T.-H. Fong, X.-G. Chen, K. K.-W. Lo, *Inorg. Chem.* **2010**, *49*, 5432–5443.
[57] C. L. Ho, K. L. Wong, H. K. Kong, Y. M. Ho, C. T. L. Chan, W. M. Kwok, K. S. Y. Leung, H. L. Tam, M. H. W. Lam, X. F. Ren, A. M. Ren, J. K. Feng, W. Y. Wong, *Chem. Commun.* **2012**, *48*, 2525–2527.

Manuscript received: July 28, 2021
Accepted manuscript online: August 11, 2021
Version of record online: October 7, 2021

